Available online at www.sciencedirect.com
SCIENCE DIRECT®
Journal of Sound and Vibration 291 (2006) 932–962
JOURNAL OF SOUND AND VIBRATION
www.elsevier.com/locate/jsvi

Vibration damping, energy and energy flow in rods and beams: Governing formulae and semi-infinite systems

G. Pavić*

Laboratoire Vibrations-Acoustique, Institut National des Sciences Appliquées de Lyon, 20, avenue Albert Einstein, 69621 Villeurbanne, France

Received 19 December 2003; received in revised form 20 May 2005; accepted 4 July 2005
Available online 12 September 2005

Abstract

Generic features of energy and energy flow in thin rods and beams are investigated. Full equations of energy density and energy flow are formulated in terms of wave amplitudes. The differential equations for energy and energy flow are also formulated which are similar but not identical to some found earlier. The relationship between the power input and global kinetic and potential energies has been applied to rods and beams which gives easy access to their global energy. The present study is focused on semi-infinite rods and beams, and in particular, at the distribution of kinetic and potential energies within the section between the excitation and the end positions. A study of a finite beam system is presented in a companion paper.

Both force and moment-type excitations are considered. It is shown that long finite beams closely match equivalent semi-infinite beams, where frequency band-averaged energy characteristics are concerned. Similar equivalence with infinite beams was found not to hold. It is further demonstrated that, unlike the kinetic energy density, the potential energy density exhibits a jump at the excitation point of a rod or a moment-driven beam. The damping was shown to reduce the jump in potential energy across the excitation point, but in turn increases the frequency range of strong power input to the end section.

*Tel.: +33 4 724 380 80/+33 4 724 387 07; fax: +33 4 724 387 12.
E-mail address: pavic@lva.insa-lyon.fr.

0022-460X/$ - see front matter © 2005 Elsevier Ltd. All rights reserved.
doi:10.1016/j.jsv.2005.07.021

1. Introduction

One-dimensional vibration objects such as axially vibrating rods and flexurally vibrating beams have been investigated thoroughly in the past. Some of these investigations were related to energy of these simple structures with two principal objectives in mind: (1) measurement of energy flow for the purpose of vibration path identification and ranking and (2) simplified modelling of energy density and energy flow with the aim of improving prediction of vibration levels at medium and high frequencies.

Following an early study of energy flow in beams and plates [1], several energy flow measurement methods emerged using either a finite-difference formulation [2–4], or a wave separation technique [5–7]. These investigations focused on a single type of vibration, mainly flexural vibration. Techniques of simultaneous measurement of several types of waves in beams were also examined, e.g. in Refs. [8,9]. It has been clearly shown that energy flow measurement techniques are intrinsically delicate and susceptible to errors. A particular difficulty related to flexural vibration was found to be the presence of a near-field which had either to be disregarded, at the cost of losing access to lower frequencies as well as regions close to discontinuities, or to be taken into account at the price of enormous loss of accuracy. Improvements of different sorts were attempted in this respect, e.g. by using hybrid formulations [10], or hybrid transducer configurations [11], but the practical problems associated with the exact positioning and amplitude-phase matching of transducers remained a major obstacle. Some notable attempts to further improve the measurements were done on the side of signal processing [12,13], showing some promising perspectives. Nevertheless, measurement of energy flow in a beam in all but well-controlled laboratory conditions is still impractical. Researchers are thus left for the time being without a potentially powerful tool which can be used not only for identification purposes but also in vibration control work [14].

Investigations into the methods of prediction of vibration of rods and beams were carried out in parallel with the development of measurement methods. Taken on its own, a thin rod or a Bernoulli–Euler beam is a simple enough object to be readily computed using analytical methods. Where assemblies of beams are concerned the analytical approach becomes too demanding while the numerical techniques such as FEM remain limited in frequency. This explains the interest in simple prediction methods which, like Statistical Energy Analysis (SEA), apply local space averaging to achieve simplicity but which, contrary to SEA, can provide some insight about how the vibrations are distributed within each subsystem, i.e. each beam.

First studies on high-frequency modelling of beams appeared in the seventies [15,16]. It has been found that the smoothed energy distribution could be represented by equations analogous to that of heat conduction. The theoretical formulations developed were implemented numerically using finite element technique [17,18]. A more detailed analysis of rods and beams has revealed that while the energy in rods does behave in accordance with heat transfer analogy the same does not apply to beams unless further local spatial averaging is applied [19].

In Ref. [20] Carcaterra and Sestieri have shown that the heat transfer analogy does not apply in the general case to vibrating mechanical systems. Lase et al. have developed an exact differential representation of energy distribution in rods and beams [21]. In the case of rods one pair of differential equations are obtained, one for total energy density and one for Lagrangian density. In the case of beams four pairs of such energy equations are needed: one pair for propagating

waves, one pair for evanescent waves and two pairs for describing the interactions between the two types of waves. The general energy formulation of Lase et al. [21] explicitly expresses the energy density in terms of smooth and oscillating components. Le Bot has concentrated on the smoothly varying part by simplifying the cumbersome general expressions [22]. A major problem of these techniques represents the specification of energy and energy flow connectivity conditions at the subsystem interfaces and across joints. Cho et al. have used superposition of incident and scattered energy densities at the discontinuity to enforce connectivity [23]. Still, the lack of simple energy connectivity laws remains a major obstacle to the use of smooth formulations.

Novel hybrid prediction methods have been recently considered to bridge the limitations of classical numerical techniques limited to lower structural modes and statistical techniques suffering from poor spatial resolution. These methods are potentially suitable for modelling of structures which involve rods and beams. In Ref. [24] Soize has proposed a technique which treats an assembled system as being composed of a master structure, dictating the overall response, and a number of attached subsystems with uncertain (fuzzy) properties. Another formulation having some resemblance to Ref. [24] was developed by Langley and Bremner, where the dynamic movements of an assembly are split into a global and a local set of degrees of freedom [25]. The two sets are then treated in different ways: the global set deterministically and the local set by some statistical or smooth formulation, like SEA. Yet another approach was proposed by Mace and Shorter [26] which also uses splitting the system into global and local subsystems, both of which are treated by FE techniques. Frequency averaging is applied. The advantage of the approach in Ref. [26] is that it can handle systems up to higher frequencies than classical FE with improved numerical efficiency arising from appropriate mathematical manipulations of the governing equations.

The objective of this paper is to provide an account of physical aspects of energy and energy flow distribution in rods and beams and in particular of the role damping plays on these quantities. With this objective in mind, the investigation will be carried out using simple analytical models of rods and beams, both infinite and semi-infinite. Finite structures are more difficult to analyse in a generic sense; an analysis focused on a particular finite system is done in a companion paper [27].

Any infinite or semi-infinite structure is of course only a theoretical concept. Nevertheless, a large real structure excited far from its boundaries if sufficiently damped will have averaged properties similar to those of an equivalent infinite one. Likewise, a large damped real structure excited close to one boundary will have averaged properties similar to those of an equivalent semi-infinite one. In fact a semi-infinite rod/beam driven in the vicinity of its end is a suitable example for studying some fundamental effects of damping on vibration energy propagation as, unlike an infinite or a finite structure, it shows effects of amplification by both wave interference and steady decay. The relevance of semi-infinite structures for vibration analysis was demonstrated by Liang and Petersson in Ref. [28]. They have found that a quantity called motion transmissibility, shown to be useful in analysing a finite structure, could be obtained by considering an equivalent semi-infinite structure. The energy equivalence of semi-infinite and finite structures will be demonstrated at the end of this paper.

Three physical quantities will be considered: kinetic and potential energies and energy flow (called sometimes power flow). The energies will be considered either locally as energy density, i.e. energy per unit length, or globally. Some attention will be paid to the distribution of potential

energy density since this quantity, shown to be directly related to local energy losses, can serve as an indicator of the locations of high damping effect and thus could be used in vibration control optimisation.

Yet another quantity becomes relevant for energy analysis, the energy flow divergence. The flow divergence has been found to be proportional to potential energy density [29]. It is therefore unnecessary to consider both the potential density and the flow divergence. The choice between the two will be made in dependence of the nature of the analysis.

2. Energy and energy flow in a continous system

This section recalls some basic relationships between the local and global distribution of energy and energy flow of a vibrating system in the presence of structural damping. The system considered is supposed linear. Sinusoidal time variations with frequency ω are assumed which allows taking all the time variables as complex quantities. Only the time-averaged values of energy and energy flow (intensity) are investigated.

Both energy and energy flow are linear combinations of products of stresses, strains and velocities. It is well known that the time-averaged product of two harmonically varying quantities u_1 and u_2, represented in complex form, is numerically equal to the real part of the product of their complex amplitudes U_1 and U_2

$$\overline{u_1(t)u_2(t)} \hat{=} \frac{1}{2}\,\mathrm{Re}\{U_1 U_2^*\},$$

where overbar denotes time average, asterisk denotes complex conjugate and Re denotes real part. Once the complex product $U_1 U_2^*$ is available, it becomes useful to employ not only its real part but its imaginary part as well in spite of the physical meaning of the latter being usually obscure. The time-averaged product can then be taken as complex. In the rest of the paper the time-averaged energy flow (power) will be considered to be a complex quantity, while the energy will be considered as a purely real quantity.

The divergence of the complex intensity vector I within an elastic structure has been shown to depend on energy density e and loss factor η in the following way [29]:

$$\nabla \cdot \bar{I} = \mathrm{Re}(\nabla \cdot \bar{I}) + \mathrm{j}\ \mathrm{Im}(\nabla \cdot \bar{I}) = 2\omega\left[(\mathrm{j} - \eta)\bar{e}_p - \mathrm{j}\bar{e}_k\right], \tag{1}$$

where e_k and e_p denote the kinetic and potential energy densities, respectively, i.e. the energy per unit volume while the symbol Im denotes the imaginary part. Eq. (1), used in a somewhat modified form in Ref. [22], applies not only to one-dimensional structures, but to arbitrary linear systems with structural damping [29]. The integral representation of Eq. (1) then is given in terms of total system energy and input power [29]

$$\overline{P}_{\mathrm{in}} = 2\omega\left[\mathrm{j}\overline{E}_k + (\eta - \mathrm{j})\overline{E}_p\right]. \tag{1a}$$

Eqs. (1) and (2) hold strictly at all frequencies. The only restriction is the assumption on the loss factor which has to be constant throughout the body if Eq. (2) is to stay valid. Eq. (1) shows that the net divergence of energy flow in a steady state of vibration is proportional to the potential energy.

3. Energy and power distribution in rods

3.1. Basic relationships

A straight rod vibrating in the axial direction is perhaps the simplest continuous system to analyse. Yet it will be shown that the laws governing energy and its flow are far from being very simple.

The rod is supposed to vibrate in a longitudinal direction such that the distribution of strains over the cross-section is uniform. The usual form of solution in the case of harmonic motion of a lossless rod of elasticity modulus E and mass density ρ given in terms of axial displacement u reads

$$u(x,\ t) = U(x)\mathrm{e}^{\mathrm{j}\omega t}, \qquad U = A_{+}\mathrm{e}^{-\mathrm{j}kx} + A_{-}\mathrm{e}^{\mathrm{j}kx}. \tag{2}$$

Here $A = |A|\mathrm{e}^{\mathrm{j}\varphi}$ denotes complex amplitudes of oppositely propagating longitudinal waves while ω denotes angular frequency. In the absence of damping the wavenumber k becomes a real quantity

$$k = \omega/c, \quad c = \sqrt{E/\rho} \tag{3}$$

c representing propagation velocity. In such a case the energy flow through the rod per unit cross-sectional area, the intensity, becomes proportional to the difference in the amplitude squares of the two waves

$$I = \frac{1}{2}\sqrt{E\rho}\omega^2\left(|A|_{+}^2 - |A|_{-}^2\right). \tag{4}$$

An equation of type (4) represents a basic expression for intensity in vibration and acoustics where non-dispersive undamped plane waves are concerned. By neglecting the, often unimportant, evanescent wave field, an analogous expression becomes valid for the case of undamped flexural waves. The energy flows of the two wave types add algebraically, wave interference does not take place. However, the presence of damping will modify the nature of this simple expression, Appendix A.

The basic energy expressions are given by Eqs. (A.2)–(A.9). While the kinetic and potential energy densities vary considerably along the rod, the total energy varies slowly in an exponential fashion. The net energy flow also varies slowly, but the imaginary part of the flow, just like the kinetic and potential energies, oscillates at the rate of two periods per wavelength. The equation of total energy density given in terms of wave amplitudes (A.4) yields the following differential equation for energy [21]:

$$\frac{\partial^2\overline{E'}}{\partial x^2} - (\eta k)^2\overline{E'} = 0, \tag{5}$$

which is universally valid, i.e. at all positions and frequencies. Such an equation, already found by Wohlever and Bernhard in Ref. [19] and termed "approximate", uses an approximate equation of energy flow free from an interference term. This nevertheless produced the exact solution for E' since total energy density, contrary to energy flow, is interference free. If subjected to appropriate boundary conditions (5) will produce an exact result for energy distribution in an axially vibrating rod.

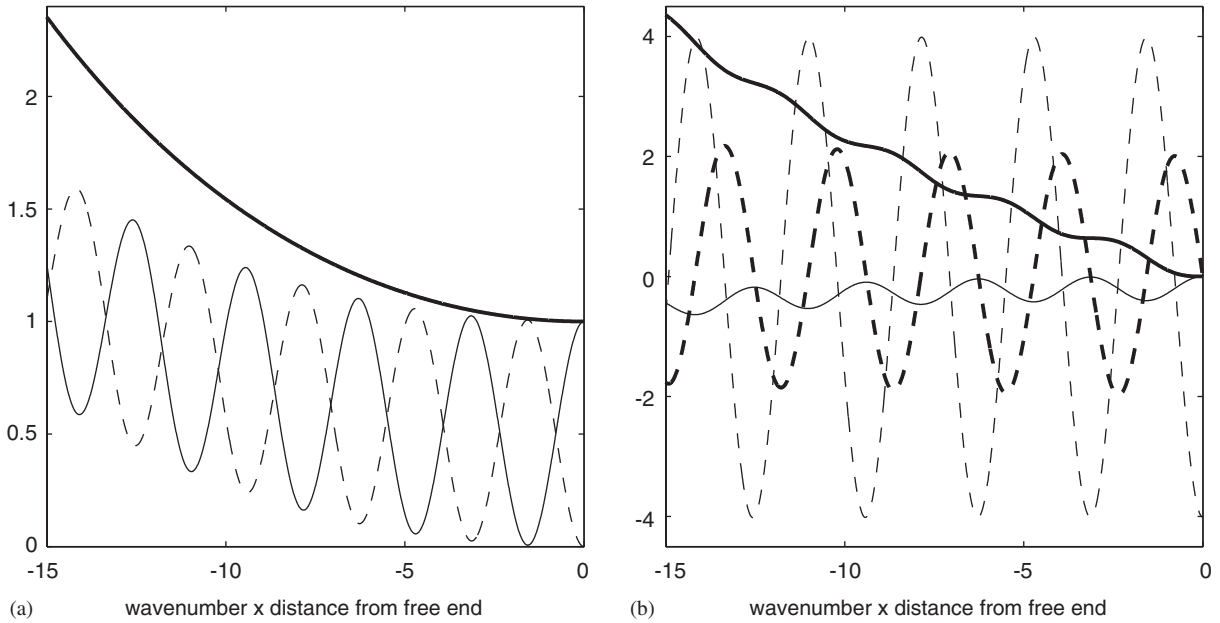

Fig. 1. Normalised energy density (a) and energy flow (b) of a rod having one end free at $x = 0$. (a) —— total, —— kinetic, - - - potential; (b) —— real flow, —— imag. flow, - - - real divergence; - - - imag. divergence.

To outline the nature of energy distribution in rods, the rod will be assumed to be free at the end $x = 0$. This condition implies zero potential energy and zero net energy flow which in turn will yield the following laws of energy distribution:

$$\overline{E'_k} \propto \cosh(\eta kx) + \cos(2kx), \quad \overline{E'_p} \propto \cosh(\eta kx) - \cos(2kx),$$
$$\overline{P} \propto -(1 + \mathrm{j}\eta/2)[\sinh(\eta kx) + \mathrm{j}\sin(2kx)],$$
$$\nabla(\overline{P}) \propto -(1 + \mathrm{j}\eta/2)[\eta\cosh(\eta kx) + 2\mathrm{j}\cos(2kx)].$$

Fig. 1 shows the normalised energy distribution in a rod having a free end at $x = 0$, represented by the equations above. The loss factor is set to 0.1 to emphasise spatial variations. Rapid changes of kinetic and potential energy strictly cancel out to give a smooth change of total energy. An identical distribution can be obtained for another classical conservative end condition, rigid clamping, if the plots of kinetic and potential energies are interchanged.

While the variation of net energy flow is monotonic, as expected, it is not smooth: the net energy flow is staircase shaped: descents and "plateaus" appear in succession along the rod. This type of distribution is typical of damped waveguides: similar patterns will be found later in beams. On the contrary all the energy-related quantities in an infinite damped rod decrease smoothly.

3.2. *Infinite rod*

Prior to any further analysis it is helpful to find the solution for a rod extending to infinity at both sides of the excitation point. The solution for an infinite rod is available in textbooks for

damping-free conditions. The damped solution is readily obtained from Eq. (2) by imposing at the excitation point, taken here at $x = 0$, the condition $-SE\,\partial u/\partial x = F/2$, where F is the complex excitation force

$$u(x) = A_0 \mathrm{e}^{-\mathrm{j}k|x|}, \quad A_0 = \frac{F}{2\mathrm{j}m'c\omega}. \tag{6}$$

The presence of damping is taken into account by making the Young's modulus E—and thus the velocity c—complex. The power in the rod is easily obtained from Eq. (A.5) by setting A_- to zero

$$\begin{aligned}\overline{P} &= \frac{1}{2}m'c\,\omega^2(1+\mathrm{j}\eta/2)\left|A_+^2\right|\mathrm{e}^{-\eta k|x|} \\ &= \mathrm{sign}(x)\frac{\left|F^2\right|}{8m'c}(1+\mathrm{j}\eta/2)\mathrm{e}^{-\eta k|x|}.\end{aligned} \tag{7}$$

The sign(x) results from interchanging A_+ and A_- for $x<0$, resulting from the anti-symmetry of the displacement gradient field corresponding to the internal force. The input power is

$$\overline{P}_{\mathrm{in}} = 2\overline{P}\big|_{x=0} = \frac{\left|F^2\right|}{4m'c}(1+\mathrm{j}\eta/2). \tag{7a}$$

With the known complex input power the global values of kinetic and potential energies can be easily found using the integral formula (1a). It turns out that the two energies are equal within the margins of η^2.

At this point a suitable normalisation value of energy density will be introduced. As the mean energy density in an infinite rod is zero, an appropriate density reference value can be obtained by considering the section of the rod around the excitation point which contains one half of the global energy. This section can be easily identified using the integral relationship (1a): it turns out that the net power leaving this section has to be equal to half the net input power (7), (7a). The distance from the excitation point Δ at which the input power entering one side of the rod drops to half its value can be found from the condition $\exp(-\eta k\Delta) = \frac{1}{2}$, i.e. $\Delta = \ln(2)/\eta k$. Twice this distance (both sides of the rod) contains one-half of the global energy, the latter being equal to $\overline{E} \approx \mathrm{Re}\{\overline{P}_{\mathrm{in}}\}/\eta\omega$, (1a). Thus

$$\overline{e}_{\mathrm{rod}} = \frac{\mathrm{Re}\{\overline{P}_{\mathrm{in}}\}}{4\ \ln(2)c} \tag{8}$$

can be considered as a characteristic energy density of a rod. In what follows this value will be used to represent the energy density in a normalised non-dimensional way.

3.3. Semi-infinite rod

The present analysis will be now focused on to a semi-infinite rod excited near its end.

In a semi-infinite rod two vibration waves will coexist in the section between the rod end and the excitation point. These waves move in opposite directions which causes rapidly varying destructive or constructive interference in dependence of the wavelength. In the part of the rod extending to infinity the wave directly excited by the source and the wave reflected from the

boundary merge into a single wave which moves away from the excitation point. The amplitude of this resulting wave decreases slowly as there is no opposite wave to create interference. If a rod is dissipation free and moreover with conservative boundary conditions, standing waves will develop within the end section at wavelengths equal to integer fractions of the excitation-end distance. Under the same conditions the outgoing wave will fully disappear reducing the net power input to zero. Thus, the presence of internal damping will affect not only the vibration levels, but also the nature of wave propagation.

The rod end will be taken to be clamped. The response will be found by a superposition based on the solution for an infinite rod (Eq. (6)). For the sake of simplicity the clamped end is placed at $x = 0$ while the excitation force is placed at $x = d$. A secondary force of equal magnitude and opposite phase to the primary excitation force will be applied to the infinite rod at the mirror position with respect to the rod end, i.e. at $x = -d$. This force, acting simultaneously with the primary force, will cancel rod motion at $x = 0$ due to the symmetry of infinite rod displacement field which fully corresponds to the required semi-infinite boundary condition.

At the origin of the infinite rod, driven by the primary force and its mirror image counterpart, the amplitudes of the two vibration waves generated by these two forces, A_- and A_+, respectively, will be equal in magnitude but of opposite sign:$A_+ = -A_- = -A_0 e^{-jkd}$. When substituted into Eq. (A.5), the last relationship yields the value of the net input power of a semi-infinite rod. This value can be further used to evaluate the global kinetic and potential energies using Eq. (1a).

Fig. 2 shows the global energy properties of a semi-infinite rod. The abscissa scale is normalised in the form of the product kd. The plot (a) shows the normalised net input power, i.e. the actual net input power divided by the net input power of an equivalent infinite rod. This plot will remain

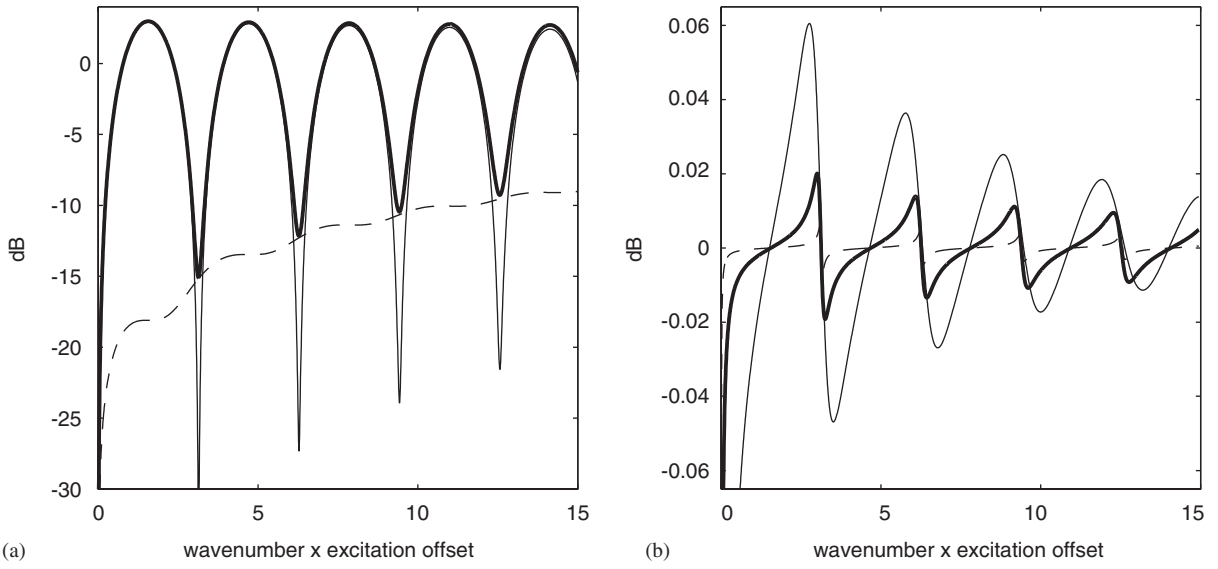

Fig. 2. Energy properties of a clamped semi-infinite rod in dependence of the wavenumber k and the distance between the excitation position and the clamped end d: (a) normalised values of net input power; thick line: at the input, thin line: transmitted to the infinite part, dashed line: transmitted to the clamped section and (b) Lagrangian coefficient; loss factor: thick line: medium (1%), thin line: high (10%), dashed line: low (0.1%).

unchanged if the potential energy is shown, as implied by Eq. (1a). The plot of kinetic energy will be practically the same as the difference between the kinetic and potential energies, the Lagrangian energy, is small. The ratio of Lagrangian energy and the total rod energy, named the Lagrangian coefficient, is shown on the plot (b) at three values of loss factor: 0.1%, 1% and 10%.

The input power and thus the global energy vary a lot with the wavenumber (frequency). It can be shown that the higher the damping the smaller the variations; with kd increasing the result converges to that of an infinite rod as expected. At $kd = n\pi$, n integer, the rod energy is at a minimum and is transferred essentially to the clamped section as seen by the dashed line. The envelope values of input power are $1 \pm e^{-\eta kd}$ which is easily found from Eq. (A.6). It follows that at low frequencies the input power to the clamped semi-infinite rod can almost double that of an infinite rod. The low values of Lagrangian coefficient at all, but very low frequencies indicate equal sharing of total energy between potential and kinetic energies. At extremely low frequencies the (clamped) rod is deformed at practically no motion, thus the potential energy prevails.

One can notice that, contrary to the case of finite systems, the energy and power input do not show peaks which are characteristic of resonances, but show instead dips at certain values of kd. These values are $n\pi$, where n is an integer. It can be readily shown that these values represent anti-resonances of the driving point located at the free end of a clamped–free finite rod. As the impedance of the infinite rod section is a smooth function of frequency, the anti-resonances of the whole semi-infinite clamped rod will coincide with those of such a finite rod. At an anti-resonance frequency of the driving point the work provided by the external excitation is almost entirely delivered to the clamped section the impedance of which is much higher than that of the infinite section at this frequency. The energy is trapped in the clamped section with very little energy leaking to the infinite section. This effect will occur no matter what is the boundary condition providing it is a conservative one: in such a case there will always be anti-resonances at some frequencies.

The impedance of the driving point can never be very low since the resistance (the real part of the impedance) of the infinite section is not negligible, which means that resonances cannot develop in semi-infinite waveguides. Damping thus affects little the input power except in frequency bands where the major part of the input power enters the clamped section. In an elastic system damping becomes effective when the inertial forces compensate the elastic forces, which occurs at resonance. The energy of an infinite rod or an infinite beam is in fact also affected by damping: vibration of a damped infinite rod decays with the distance from excitation while it does not decay if the damping is zero. However, in view of the absence of resonances, i.e. reflected waves, it does not matter much how rapid the spatial decay is, i.e. how large is the damping, provided it is not very high. In a semi-infinite rod the damping will not affect the net input power if the main energy flow is towards the infinite section, but will matter once the flow goes mainly to the finite section.

With the values of wave amplitudes identified, the energy density and intensity can be evaluated from Eqs. (A.2)–(A.5). Fig. 3 shows these quantities in the form of a tone map in dependence of frequency (wavenumber) and observation position x. Representation of a function of two variables—position along the rod (abscissa) and wavenumber (ordinate)—by a tone map is done here for the sake of giving an easy perception of the overall behaviour of the given function which depends on two parameters. Such a condensed representation will be again used in the next section dealing with beams. Both abscissa and ordinate scales are normalised in such a way to

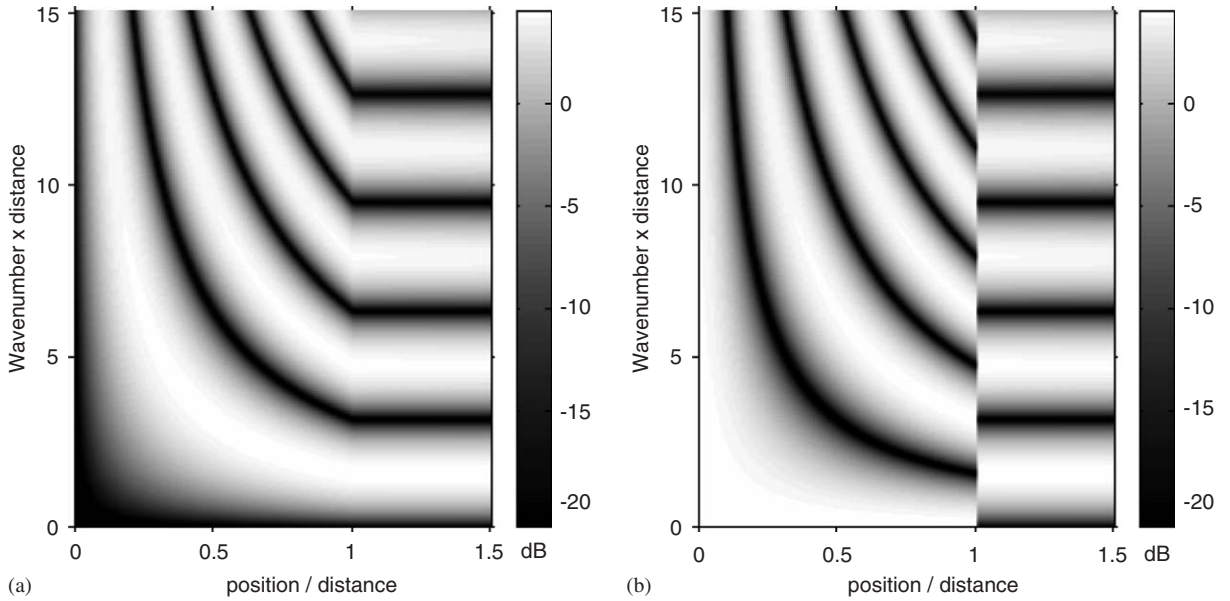

Fig. 3. Normalised energy density of a point-force-driven clamped semi-infinite rod as a function of scaled observation position (abscissa) and frequency (ordinate): (a) kinetic and (b) potential energy density. Loss factor 1%.

make the results universally applicable to any value of excitation position d. The abscissa is represented in a non-dimensional form, by the ratio of the observation position and the end-excitation distance x/d. The end thus corresponds to 0 while the excitation point corresponds to 1. The ordinate is non-dimensional too, given in Helmholtz units.

Each map is normalised by dividing the actual values of energy density by the characteristic density (Eq. (8)). The role of normalisation is not merely to make the results non-dimensional but rather to enable a better insight into the nature of energy distribution. The present study concerns the energy distribution within the system analysed, thus it appears that the most meaningful way of normalising the actual energy densities should go via some reference density, like that of an infinite rod. Such a normalisation gives unique results for any combination of the two non-dimensional entry parameters.

Regretfully the structure damping cannot be normalised in a suitable way. The damping affects the two wavenumbers of energy distribution in a non-proportional way (one wavenumber is greatly affected, the other is not). The damping should thus be considered as an independent input parameter.

It can be seen that strong variations of energy variables occur only at the positions between the rod end and the excitation point, i.e. between 0 and 1. The kinetic (a) and potential (b) energy densities in this region are seen to be different but complementary. The difference is strong near the excitation point and the clamped end, fading away toward the interior of this section. The complementary feature of the two energies can be shown by the sum of the two: at a given frequency, the total energy density in the clamped section is constant. The same feature will be displayed by any one-dimensional dispersion-free field, such as the sound field in a tube below the

first cut on. On the contrary, a beam vibrating in flexure has a very uneven distribution of total energy density as shown in Section 4.

Fig. 3 shows yet one characteristic feature which applies to both rods and beams: at the two sides of the excitation point the potential energy densities could be very different from each other. In the general case there will always be a jump, either positive or negative, in potential energy density across the excitation point at each frequency. The jump, caused by a jump in internal stresses which are responsible for potential energy in a rod, is due to the external force being unevenly split on two adjacent faces of the cross-section. It will occur whenever the rod is not symmetric with respect to the excitation point. The jump can never occur in the kinetic energy density as this quantity, being governed by the rod velocity, is a continuous function of space. It can be shown that the jump effect is preserved when the boundary condition is changed. This feature can be of importance when deciding on the placement of damping in structures: it should be always placed at positions of higher potential energy.

4. Energy and power distribution in beams

4.1. Basic relationships

In the case of a straight beam vibrating in flexure, the two travelling waves of complex amplitudes A_+ and A_- are accompanied by two evanescent ones of complex amplitudes C_+ and C_-

$$U(x,t) = \left(A_+ \mathrm{e}^{-\mathrm{j}kx} + A_- \mathrm{e}^{\mathrm{j}kx} + C_+ \mathrm{e}^{-kx} + C_- \mathrm{e}^{kx}\right)\mathrm{e}^{\mathrm{j}\omega t},$$
$$k = \left(m'/B\right)^{1/4}\sqrt{\omega}, \tag{9}$$

where B and m denote flexural stiffness and unit-length mass while $C = |C|\mathrm{e}^{\mathrm{j}\psi}$ denotes the complex amplitude of an evanescent wave. If the damping is zero, the net active energy flow expressed in terms of wave amplitudes reads [2]

$$\mathrm{Re}(\overline{P}) = \frac{m'\omega}{k}\left[\left|A_+^2\right| - \left|A_-^2\right| - \left|C_+\right||C_-|\sin(\psi_+ - \psi_-)\right], \tag{10}$$

i.e. it involves the evanescent waves too, even though each of these waves does not carry power on its own when taken individually.

The damping can now be included by making the flexural stiffness complex

$$B \to B(1+\mathrm{j}\eta) \Rightarrow k \to k/(1+\mathrm{j}\eta)^{1/4} \approx k(1-\mathrm{j}\eta/4). \tag{11}$$

With the damping included, the expression for energies, energy flow and its divergence become exceedingly complicated. These are given in Appendix B explicitly in terms of wave amplitudes just like in the case of rods in Section 3. These contain 10 different products of wave amplitudes as already shown in Refs. [21,22] and, unlike Eq. (10), depend on the observation point x

$$\overline{E}_k, \overline{E}_p, \overline{P}, \mathrm{div}(\overline{P}) = f\{x, \left|A_+^2\right|, \left|A_-^2\right|, \left|C_+^2\right|, \left|C_-^2\right|, A_+A_-^*, C_+C_-^*,$$
$$A_+C_+^*, A_+C_-^*, A_-C_+^*, A_-C_-^*\}.$$

To illustrate the complexity of energy propagation in a damped beam consider the case of a single flexural wave impinging a non-conservative boundary, such as a dissipative joint. In the general case such a wave will produce two reflected waves, one propagating and one evanescent. If the beam is lossless, Eq. (10) applies. When the incoming wave is a propagating one, the energy flow will be governed by the difference of the incoming and reflected propagating wave amplitude squares, just like in the case of air-borne sound waves. In this case the reflected evanescent wave will not participate in energy transport. If the incoming wave is an evanescent one, the net flow will still exist contributed to by both the evanescent waves and by the reflected propagating wave. However, if the beam possesses some internal dissipation the simple equation (Eq. (10)), is no longer valid. In such a case any wave arriving at a non-conservative boundary will produce energy flow which will be contributed by all the inbound and outbound waves, (Eqs. (B.3), (B.3a)).

Practical implementation of simple models of beam vibration favours use of an energy differential equation which, subjected to appropriate boundary conditions, would provide the solution for energy distribution within the beam. In Ref. [19] the authors have used an approximate second-order equation, analogous to the rod equation (5). This equation disregarded not only the evanescent wave contribution, which made it inapplicable to near-field conditions, but also the coupling between propagating waves which is responsible for the oscillatory component of energy. As a result, an approximation of beam energy density was obtained, such that energy oscillations were smoothened out.

The energy and energy flow divergence in the beam are governed by G_r and G_i terms, (Eq. (B.4a)), the first representing the propagating and evanescent fields separately, the second representing their interference. Each of the two can be put in a differential form (η^2 neglected in comparison with unity except in the expression for G_i, where it matters for the balance of the sum of all terms)

$$\frac{\partial^8 G_r}{\partial x^8} - 16k^4 \frac{\partial^4 G_r}{\partial x^4} + \eta^4 k^8 G_r = 0, \quad \frac{\partial^8 G_i}{\partial x^8} + 8k^4 \frac{\partial^4 G_i}{\partial x^4} + 16\left(1 - \frac{\eta^2}{4}\right) k^8 G_i = 0. \tag{12}$$

Each differential equation yields 4 pairs of roots. The energy flow is governed by S_+ and S_- terms which obey differential equations of the same form as Eq. (12). Thus kinetic energy, potential energy, energy flow and energy flow divergence can all be represented by 2 terms or alternatively by 8 simple terms as shown in Ref. [21]. However, the total energy is proportional only to the G_r term, i.e. free from interference between dissimilar wave types. It can be thus expressed by a single differential equation of eighth order, the same as the Lagrangian energy which is proportional to the G_i term only. As the energy flow cannot be reduced to the same order, it is not possible to establish a straightforward link between the energy flow and total energy density. The complete energy density equation will be consequently of little practical use. It should be pointed out that Le Bot has obtained for the total and Lagrangian energy a system of two coupled differential equations of eighth order which stands in some contrast to the result (12) where the two are uncoupled.

By neglecting the evanescent terms C_+ and C_- in the energy equation (B.6), an approximate differential-averaged energy equation can be reached. The energy variation is governed by one harmonic term at the rate $2kx$ and two oppositely decaying terms at the rate $\eta kx/2$ which results in

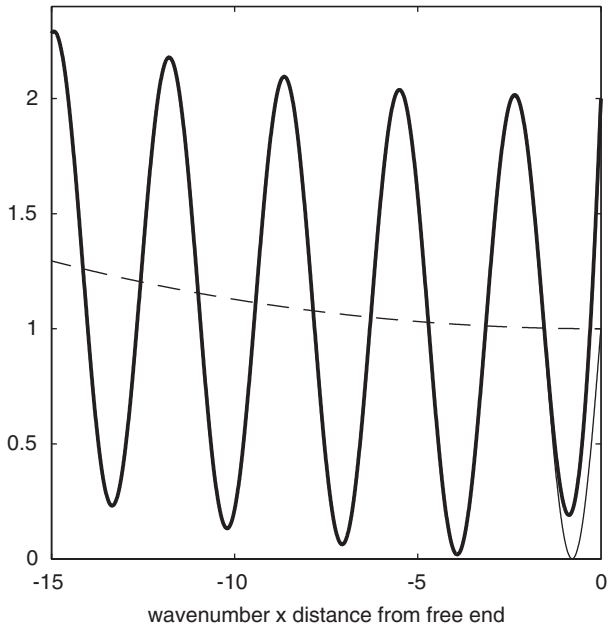

Fig. 4. Normalised total energy density in a beam with one end free. Loss factor 1%. —— exact; —— approximate; – – – simplified.

a fourth-order differential energy equation

$$\frac{\partial^4 \overline{E'}}{\partial x^4} + 4k^2\left(1 - \frac{\eta^2}{16}\right)\frac{\partial^2 \overline{E'}}{\partial x^2} - \eta^2 k^4 \overline{E'} = 0. \tag{13}$$

This equation now contains only 4 unknowns and thus requires 4 boundary conditions. It will well describe the spatial variations of total energy at all positions except near the beam ends where the influence of the near-field could be strong. This will inevitably make Eq. (13) unsuitable for modelling of built up systems which relies heavily on the accuracy of representation of boundary conditions.

Fig. 4 shows the distribution of total energy near a free end of a beam, $x = 0$. The thick curve shows the exact value (Eq. (B.6)), the thin curve shows the approximate value obtained by neglecting the near-field (Eq. (13)), while the dotted curve represents the simplification used in Ref. [19]. It can be seen that the approximation (13) is globally quite satisfactory. Of course this approximation cannot be applied in the computation of beam assemblies by energy equations but can be employed for the experimental analysis of far-field regions.

4.2. *Infinite beam*

A simple academic case of an infinite beam will be briefly analysed as an introduction to a more general analysis. Moreover, the results of this section will be employed in the following section to analyse the response of a semi-infinite beam. It will be shown that, even in the exceptionally simple

case of an infinite beam excited at a single point, the energy distribution along the beam as well as energy flow through it varies spatially in a way which is not self-evident. In particular, the rate of absorption of vibration energy away from the driving point does not decrease steadily. The case of an infinite beam has been treated in textbooks such as Ref. [30], but by neglecting damping which explains the present introduction.

Both force and moment excitation will be considered. The latter, often neglected in analysis, was shown to be of the same significance as the former [31]. In particular, the importance of power injection by moment excitation with rising frequency has been clearly demonstrated.

The beam is extended to infinity at both sides from the excitation position taken at $x = 0$. In such a case the vibration displacement field is either symmetric (force excitation) or asymmetric (moment excitation). At each side of the excitation point only two waves exist, one propagating and one decaying. For $x>0$, these two waves have complex amplitudes A_+ and C_+ using the notation of Eq. (9). The boundary conditions applied to sinusoidal vibrations yield the following values of wave amplitudes in the part $x>0$:

$$\begin{aligned} \text{force excitation}: &\quad A_+ = \frac{F}{4\mathrm{j}Bk^3}, \quad C_+ = -\mathrm{j}A_+, \\ \text{moment excitation}: &\quad A_+ = \frac{M}{4Bk^2}, \quad C_+ = -A_+ \end{aligned} \tag{14}$$

with F, M, B and k complex. The complex power input to an infinite beam can be easily evaluated from the last expressions neglecting the higher powers in η

$$\begin{aligned} \text{force excitation}: &\quad \overline{P}_{\text{in}} = \frac{(1-\eta/4)+\mathrm{j}(1+\eta/4)}{8k\sqrt{Bm'}}\left|F^2\right|, \\ \text{moment excitation}: &\quad \overline{P}_{\text{in}} = \frac{(1+3\eta/4)-\mathrm{j}(1-3\eta/4)}{8\sqrt{Bm'}}k\left|M^2\right|. \end{aligned} \tag{15}$$

The power input to an infinite beam is thus almost unaffected by damping providing the loss factor stays well below unity. This result will be generally valid for any infinite structure. It is useful to recall that the net input power to a finite structure, if averaged over a frequency band covering several resonances, should also be independent of structural damping [30], but at each particular frequency the dependence on damping is strong.

The relationship between the global energy and the excitation of the beam can be readily obtained using the integral relationship between the energy and energy flow (Eq. (1a)), as well as Eq. (15)

$$\begin{aligned} \text{force excitation}: &\quad \overline{E}_p \approx \left(\frac{1}{\eta}-\frac{1}{4}\right)\frac{\left|F^2\right|}{16\sqrt{Bm'}k\omega}, \quad \overline{E}_k \approx \left(\frac{1}{\eta}+\frac{3}{4}\right)\frac{\left|F^2\right|}{16\sqrt{Bm'}k\omega}, \\ \text{moment excitation}: &\quad \overline{E}_p \approx \left(\frac{1}{\eta}+\frac{3}{4}\right)\frac{k\left|M^2\right|}{16\sqrt{Bm'}\omega}, \quad \overline{E}_k \approx \left(\frac{1}{\eta}+\frac{7}{4}\right)\frac{k\left|M^2\right|}{16\sqrt{Bm'}\omega}. \end{aligned} \tag{16}$$

The total kinetic and potential energies of an infinite beam are almost identical. For a given excitation level, the total energy in a force-driven beam will decrease with frequency by 4.5 dB/octave while the decrease in a moment-driven beam will be much slower, 1.5 dB/octave.

The complex energy flow through the beam at an arbitrary position x in this case reads, (Eqs. (B.3), (15)):

force excitation :

$$\overline{P} = \frac{|F^2|/k}{16\sqrt{Bm'}}\left(1+\mathrm{j}\frac{\eta}{2}\right)\left\{\mathrm{e}^{-\eta k|x|/2}+\frac{\eta}{4}\mathrm{e}^{-2k|x|} + \mathrm{j}\sqrt{2}\left(1-\frac{\eta}{4}\right)\mathrm{e}^{-k(1+\eta/4)|x|}\ \cos\left[\frac{\pi}{4}-k(1+\eta/4)|x|\right]\right\}, \tag{17a}$$

moment excitation :

$$\overline{P} = \frac{|M^2|k}{16\sqrt{Bm'}}\left(1+\mathrm{j}\frac{\eta}{2}\right)\left\{\mathrm{e}^{-\eta k|x|/2}+\frac{\eta}{4}\mathrm{e}^{-2k|x|} + \mathrm{j}\sqrt{2}\left(1-\frac{\eta}{4}\right)\mathrm{e}^{-k(1+\eta/4)|x|}\ \cos\left[\frac{\pi}{4}+k(1+\eta/4)|x|\right]\right\}. \tag{17b}$$

Note that the x-coordinate appears as an absolute value due to symmetry. An expression for the net energy flow under force excitation, obtained earlier by Goyder and White in Ref. [32], fully matches the real part of Eq. (17a). The divergence of energy flow follows from Eqs. (B.4) and (15)

force excitation :

$$\mathrm{div}(\overline{P}) = -\frac{|F^2|}{32\sqrt{Bm'}}\left(1+\mathrm{j}\frac{\eta}{2}\right)\left\{\frac{\eta}{2}\left[\mathrm{e}^{-\eta k|x|/2}+\mathrm{e}^{-2k|x|}\right] + 2\mathrm{j}\mathrm{e}^{-k(1+\eta/4)|x|}\ \sin\left[k(1+\eta/4)|x|\right]\right\}, \tag{18a}$$

moment excitation :

$$\mathrm{div}(\overline{P}) = -\frac{\omega|M^2|}{32B}\left(1+\mathrm{j}\frac{\eta}{2}\right)\left\{\frac{\eta}{2}\left[\mathrm{e}^{-\eta k|x|/2}+\mathrm{e}^{-2k|x|}\right] - 2\mathrm{j}\mathrm{e}^{-k(1+\eta/4)|x|}\cos\left[k(1+\eta/4)|x|\right]\right\}. \tag{18b}$$

Both the energy flow and its divergence are composed of one slowly decaying part (the first term in brackets of Eqs. (17) and (18)), one rapidly decaying part (second term) and a harmonically oscillating part which at the same time rapidly decays (third term). The maximum is always at the excitation position, $x = 0$. The rapidly decaying part of the net energy flow can be neglected, being weighted by the loss factor. As far as the flow divergence is concerned the same term plays as important a role close to the source as the slowly decaying term.

By analysing Eq. (18) it can be found that the divergence under a force excitation will rapidly drop to $\approx \frac{1}{4}$ of its maximum value at $kx \approx 1$, only to slightly increase with increasing distance before definitely decaying towards infinity. The divergence due to moment excitation will decrease less rapidly to its first minimum value located at $kx \approx 2.4$ equal to $\approx \frac{1}{5}$ of its maximum value. In return it will assume lower relative values further away from the excitation point.

While the global values of kinetic and potential energies in an infinite beam are practically the same, their local values, i.e. the energy densities, are mutually very different though. This can be

easily seen by inspecting the expression for flow divergence (Eq. (18)), the imaginary part of which corresponds to the difference of kinetic and potential energy density according to Eq. (1).

At the excitation point, $x = 0$, the energy flow divergence is at maximum. Expressed in terms of input power via Eqs. (15) and (18a), it reads

$$\text{force excitation}: \qquad \operatorname{div}(\overline{P})\big|_{x=0} = -\frac{\operatorname{Re}\{\overline{P}_{\text{in}}\}\eta k}{4(1-\eta/4)}\left(1+\mathrm{j}\frac{\eta}{2}\right), \tag{19a}$$

$$\text{moment excitation}: \qquad \operatorname{div}(\overline{P})\big|_{x=0} = -\frac{\operatorname{Re}\{\overline{P}_{\text{in}}\}k}{2(1+3\eta/4)}(\eta-\mathrm{j}). \tag{19b}$$

For a given power input, the net divergence of energy flow provided by a moment is approximately double of that provided by a force. This implies that around the driving point the beam will absorb twice the vibration energy when driven by a moment rather than by a force at the same injected power. The latter means that the potential energy in the moment excitation neighbourhood is larger than in a force excited one. Yet the energy density at the excitation position is practically the same whether the excitation is of force or moment type as it can be found by using Eqs. (1) and (19a) and (19b):

$$\text{force excitation}: \quad \bar{e}_p = \bar{e}_k = \frac{\operatorname{Re}\{(\overline{P})_{\text{in}}\}k}{8\omega(1-\eta/4)},$$

$$\text{moment excitation}: \quad \bar{e}_p = \frac{2\operatorname{Re}\{(\overline{P})_{\text{in}}\}k}{8\omega(1+3\eta/4)}, \quad \bar{e}_k \approx 0.$$

The characteristic value of energy density in beams can be found in an analogous way to that of a rod. The approximate value of the distance from the excitation point Δ at which the net input power entering one side of the beam drops to half its value follows from $\exp(-\eta k\Delta/2) = \frac{1}{2}$, i.e. $k\Delta = 2\ln(2)/\eta$ ((17a)). Half the global energy divided by twice this distance

$$\overline{e}_{\text{beam}} = \frac{\operatorname{Re}\{\overline{P}_{\text{in}}\}}{8\ln(2)}\frac{k}{\omega} = \frac{\operatorname{Re}\{\overline{P}_{\text{in}}\}}{4\ln(2)c_g} \tag{20}$$

can thus be considered as the characteristic energy density of a beam where c_g—group velocity. Thus both rod and beam have the same characteristic energy when expressed in terms of input power and group velocity. Referring to Eq. (15) the characteristic energy density in a beam vibrating in flexure is seen to decrease with frequency at a given level of force excitation but remains independent of frequency at a given level of moment excitation.

Fig. 5 shows the normalised energy density, i.e. the energy density divided by the characteristic density as a function of distance from the excitation point expressed in Helmholtz units. The loss factor is 1%. Close to the excitation point the kinetic and potential energy densities differ a lot. The total energy density, i.e. the sum of the two decreases at first rapidly with distance from the driving point while the further decrease is much slower. Significant variations in kinetic and potential energy stay limited to approx. half the wavelength. At distances larger than half the wavelength both energies become practically the same, moreover for both types of excitation. It can be further shown that changes in damping do not modify appreciably the energy density distribution in the excitation area.

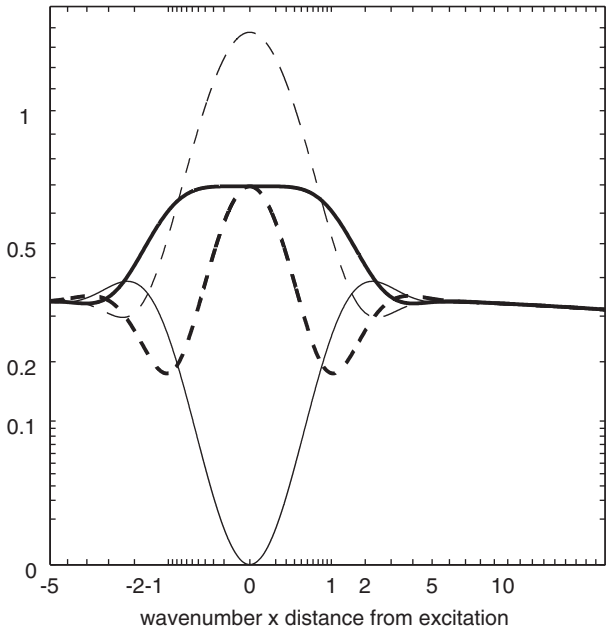

Fig. 5. Normalised energy density in an infinite point-driven steel beam. Thick line: force excitation, thin line: moment excitation. Full line: kinetic energy, dashed line: potential energy. Loss factor 1%. Axes are displayed in square root scale for improved visual resolution.

Fig. 5 indicates that damping placement at the driving point will be much more efficient if the excitation is by a moment rather than by a force. At approx. 0.17 wavelengths the potential energy due to force excitation is at a minimum; the position of the minimum is approx. at 0.38 wavelengths in the case of a moment-driven beam. Placing some external damping at these positions would consequently produce little effect on vibration reduction.

4.3. Semi-infinite beam

The present case will be now extended to the one of a semi-infinite beam excited near its end. The beam end will be taken to be clamped. The response will be found by a superposition based on the solution for an infinite beam (Eqs. (9) and (14)). The clamped end is located at $x = 0$ while the excitation force acts at $x = d$. First, a secondary force of magnitude and phase equal to the primary force will be applied to the infinite beam at twice the excitation-boundary distance, i.e. at $x = -d$. This force, acting simultaneously with the primary excitation force, will cancel rotation at $x = 0$ owing to the symmetry of an infinite beam displacement field. The remaining lateral displacement at $x = 0$ will be suppressed by an additional normal force at $x = 0$ which in turn will not create any rotation at this point (Fig. 6). As a result, the superposed fields of the primary, secondary and compensating forces acting on the infinite beam will create the same field at $x \geqslant 0$ as a single primary force acting on a semi-infinite beam clamped at $x = 0$.

Similarly, the semi-infinite beam response excited by a moment can be found by superposing to an infinite beam a secondary moment at $x = -d$ of the same magnitude and opposite phase as

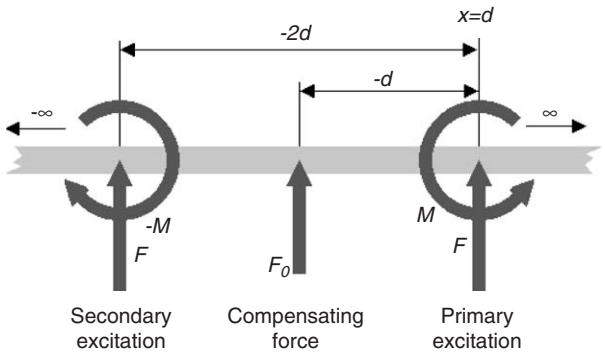

Fig. 6. Model of a clamped semi-infinite beam.

the primary moment, with the addition of a force at $x = 0$ adjusted to block the lateral motion at this point.

While the secondary excitation is exactly equal in magnitude to the primary one, the compensation force will depend on the wavenumber, and thus on frequency. Using Eq. (14) the condition of zero movement at $x = 0$ can be transformed into the following expressions for the compensation force F_c:

$$\begin{aligned} \text{force excitation}: \quad & F_c = -(1+\mathrm{j})\left(\mathrm{e}^{-\mathrm{j}kd} - \mathrm{j}\mathrm{e}^{-kd}\right)F, \\ \text{moment excitation}: \quad & F_c = (1-\mathrm{j})\left(\mathrm{e}^{-\mathrm{j}kd} - \mathrm{e}^{-kd}\right)kM. \end{aligned} \tag{21}$$

With the compensating force defined, the vibration field can be readily computed by superposition.

Each of the three excitations, primary, secondary and compensating, will create both propagating and evanescent waves. In the region $x \geqslant d$ all of the six waves from these three excitations move in the same direction, thus adding to one single propagating and one single evanescent wave. In the region between the excitation point and the boundary the waves simultaneously move in opposite directions adding up to four resulting waves. As a consequence, in $x < d$ all 10 terms of Eqs. (B.3)–(B.6) have to be used in the expressions for energy flow and its divergence, in contrast to the region $x \geqslant d$ where only 3 terms do not vanish.

Fig. 7 presents the global beam properties in dependence of kd. The figure refers to the normalised net input power but corresponds equally to the energy of the beam in view of Eq. (1a). Both cases of excitation, i.e. by force (a) and by moment (b), are displayed for easier comparison. The normalisation is made by dividing the actual values by the net input power of an infinite beam.

The dips in the energy and power input exist at certain values of kd just like in the case of a semi-infinite rod. These values are $(n+1/4)\pi$ for force excitation and $(n-1/4)\pi$ for moment excitation, where n is an integer. It can be shown that these values represent the driving point anti-resonances of a clamped–free beam excited at the free end: the first set of values corresponds to linear motion under force excitation while the second set corresponds to angular motion under moment excitation. These results follow the same reasoning discussed in Section 3 for the case of a semi-infinite rod.

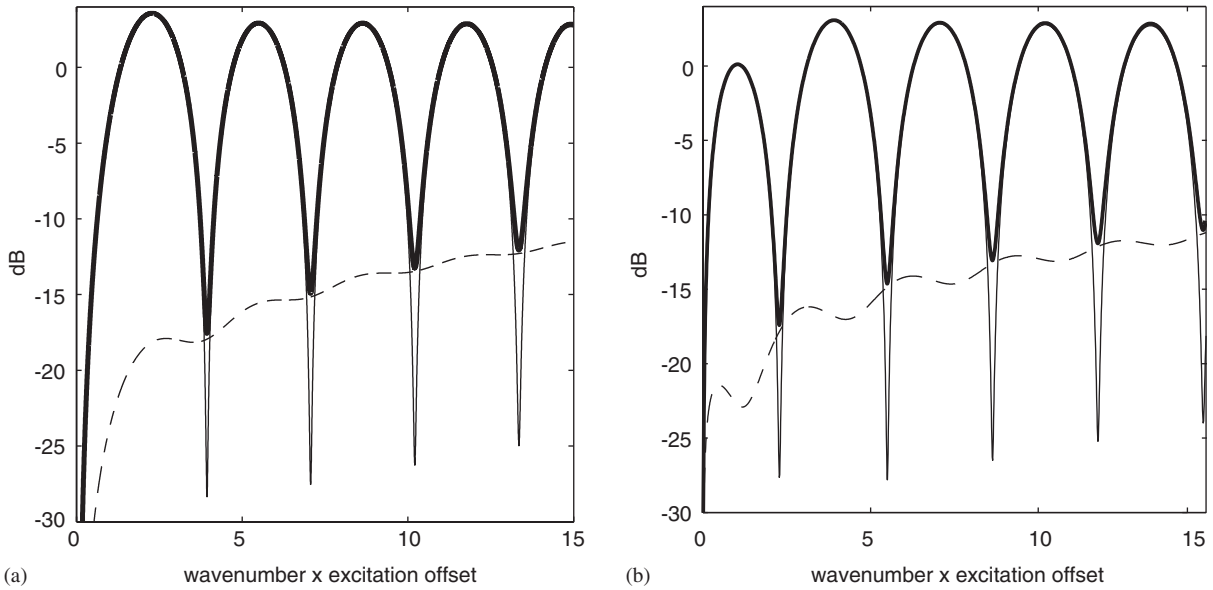

Fig. 7. Normalised input power of a point-driven semi-infinite clamped beam: (a) force excitation and (b) moment excitation. Thick line: input, thin line: transmitted to infinite part, dashed line: transmitted to the clamped section.

Fig. 8 shows the position–frequency maps of normalised energy density in a semi-infinite beam under force (a, b) and moment (c, d) excitation. Abscissa, ordinate and energy density values are all normalised the same way as in Section 3. As expected, the energy density exhibits oscillations between the excitation and end positions while globally decaying towards infinity.

Away from the excitation point in the direction of the beam extending to infinity no waves can move in the negative direction, thus no energy density oscillations are possible. This does not imply that the energy loss has to monotonically decrease: undulations are possible due to interference between the propagating and decaying waves. Far away from the excitation the decaying wave will effectively disappear and the energy loss will continue to decrease monotonically in the exponential way.

The kinetic energy is smoothly distributed at each frequency and no particular significance could be attributed to the excitation position. The potential energy exhibits a similar pattern away from discontinuities, but close to discontinuities any similarity is lost.

Fig. 9 shows the distribution of input net power between the clamped and infinite sections in dependence of damping. The values are represented in a relative way, as the ratio between the net power entering the clamped section and the net total input power. As expected, the frequency bands receiving the major part of the input power become wider as damping increases.

The jump in potential energy density at the excitation position produced by moment excitation is clearly noticeable. As noted in Section 3 a jump will always appear when the beam is not symmetrical about the excitation position. The local potential energy, proportional to the squared modulus of the internal bending moment, will exhibit a jump if the internal moments at the excitation point acting on the left- and right-hand sides of the beam are not equal in magnitude. If the beam is symmetrical, although the moment jump at the excitation point does exist, the internal

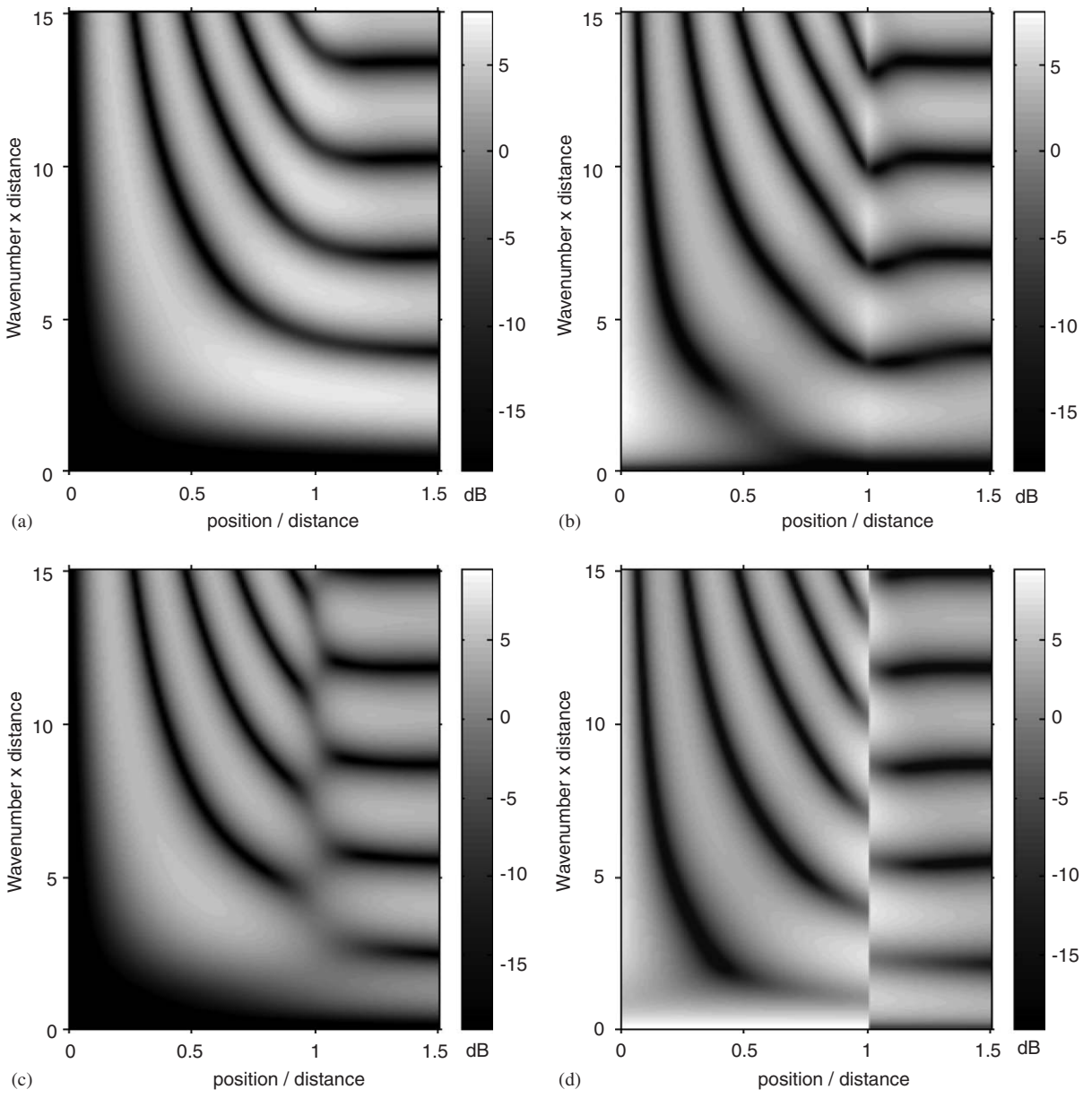

Fig. 8. Normalised energy density of a point-driven clamped semi-infinite beam: (a), (b) force excitation and (c), (d) moment excitation. (a), (c) kinetic and (b), (d) potential energy density. Loss factor 1%.

moments are of identical magnitude (equal to one half the excitation moment magnitude) thus producing no jump in the potential energy and consequently no jump in internal energy loss.

A force-driven beam cannot experience any moment jump at the excitation point, no matter whether the beam is symmetrical or not. Thus force excitation will never result in a discontinuity of energy loss across the excitation point.

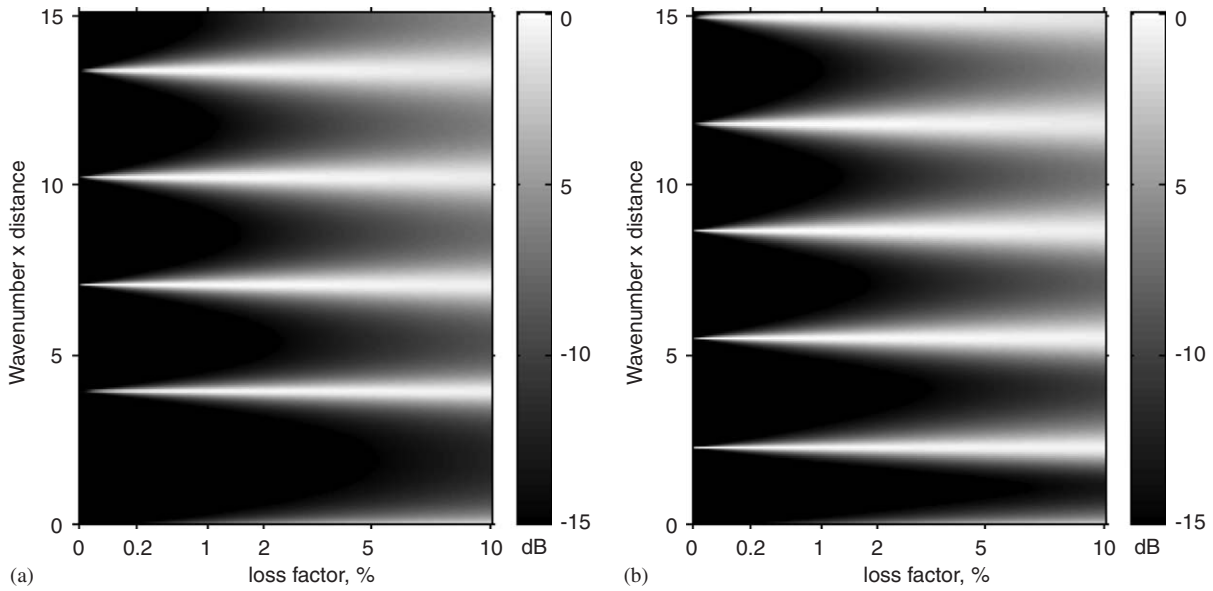

Fig. 9. Relative value of energy flow entering the clamped beam section: (a) force excitation and (b) moment excitation.

Fig. 10 shows the jump in potential energy density across the driving point of a semi-infinite moment-driven beam at different values of governing Helmholtz number. The actual value of the jump is divided by the mean value of potential energy at the driving point, taken as half the sum of the densities at the two points neighbouring the excitation point. The variations in damping are shown as shades of grey, ranging from black (zero loss factor) to light grey (loss factor 10%). The damping does not affect qualitatively the jump which just slowly shrinks as the damping increases.

It can be concluded that, given the same input power to a beam, the vibration due to moment excitation can be more efficiently suppressed than that due to force excitation by placing damping close to the excitation point.

4.4. Comparison of semi-infinite and finite beam energies

At this point it becomes useful to make a comparison between the global energy characteristics of a semi-infinite and an equivalent finite beam. Such a comparison can be meaningful if the finite beam is sufficiently long to let the vibration waves pass through several wavelengths before reaching the opposite end of the beam. For the sake of completeness the analysis will be nevertheless carried out from zero frequency. The energies of two beams will be different at each given single frequency as the finite beam has to go through resonant peaks and troughs contrary to the semi-infinite beam. Still, the global frequency behaviour of the two types of beams can be expected to match.

Skudrzyk has found that the geometric mean of the driving point mobility of a finite vibratory system corresponds to that of an equivalent infinite system [33]. It is worthwhile examining whether the same applies to the system energies. This will be done via an example, that of a beam

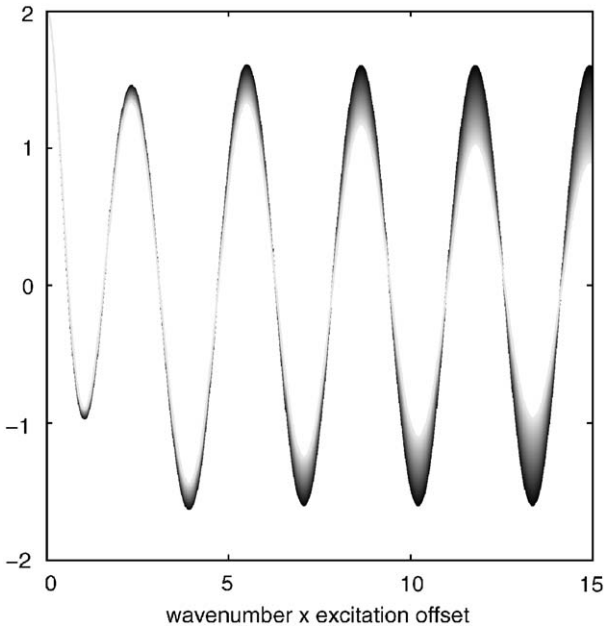

Fig. 10. Relative jump in potential energy density at the driving point under moment excitation in dependence of the wavenumber k and the distance between the excitation position and the clamped end d. Continuous linear variation of loss factor from 0% (black) to 10% (light grey).

of the same material, cross-section and damping as analysed in Section 4. Three cases will be studied: an infinite beam, a semi-infinite clamped beam driven at 1 m from its clamped end and finally a 10 m long finite clamped–free beam driven in the identical way as the semi-infinite one. The response of the finite beam will be computed using a closed solution for the beam as described in Ref. [27].

Fig. 11 shows the global energy of the three beams in dependence of frequency. The abscissa axes are presented in a square root frequency scale, i.e. in a linear wavenumber scale, to match the resonance density of the finite beam. Plot (a) corresponds to unit force excitation, the other one to unit moment excitation. It can be clearly seen that the energy of the semi-infinite beam is indeed equal to the geometric mean of the finite beam energy. The energy of the infinite beam is however very different from that of the semi-infinite beam, especially at lower frequencies.

The energy of the beam was then averaged in frequency bands. The band limits were chosen in such a way as to accommodate five resonances in each band. The eigenvalues of a cantilever of length L are given by $kL \approx (n-1/2)\pi$, $n = 1, 2, 3\ldots$, thus the band limits were set at the wavenumbers $k_n = qn\pi/L$, $n = 0, 1, 2, \ldots$, to fit midway between two adjacent resonances where q is the number of resonances per band, i.e. 5. The band limits are marked on Fig. 11 by dotted lines. Fig. 12 shows the band-averaged values of beam energy computed by taking the energy shown in Fig. 11 as a spectral density. It can be seen that the semi-infinite beam remarkably well represents the finite beam in the averaged energy sense. The differences in the averaged energy of the finite and infinite beam are not negligible though. The discrepancy is maximum at the lowest band, especially in the force-driven case (graph (a)). The discrepancy comes from the boundary

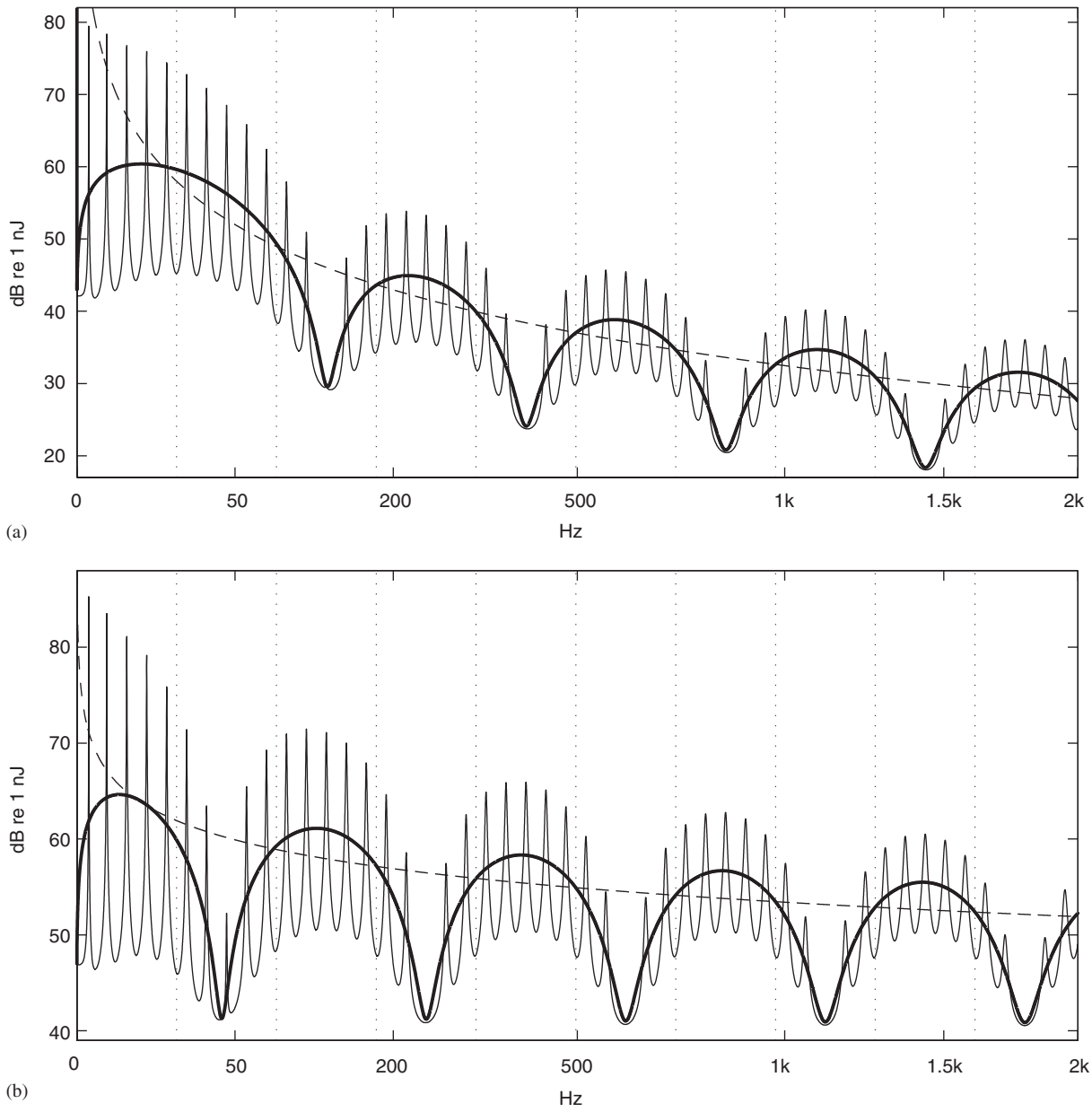

Fig. 11. Total energy of a beam vibrating in flexure: (a) force excitation and (b) moment excitation. Thin line: finite beam; thick line: equivalent semi-infinite beam; dashed line: infinite beam.

condition of the finite beam which makes its energy converge to a small value of static potential energy as the frequency falls towards zero, while the energy of the infinite beam becomes infinite in this case (Eq. (16)). But, the discrepancies between these two cases exist at high frequencies too which implies that the infinite beam is not a good representative of a finite beam in the energy sense.

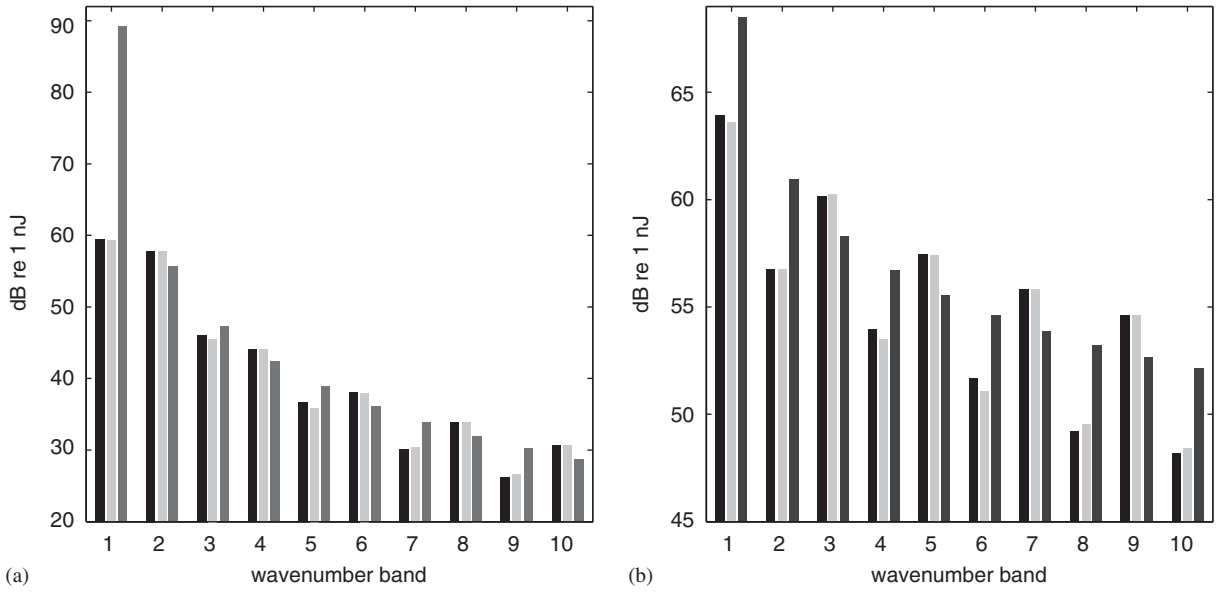

Fig. 12. Band-averaged spectra of total energy of a finite (black), semi-infinite (light grey) and infinite (dark grey) beam: (a) unit force excitation and (b) unit moment excitation. Band limits are marked by dotted lines on Fig. 11.

The energy shown on Figs. 11 and 12 is the total beam energy. The next question is how the kinetic and potential energies of the three beams analysed match in a frequency-averaged sense. This will be examined by comparing the Lagrangian coefficients of these beams. The Lagrangian coefficient is presented on Fig. 13. Again the semi-infinite beam is seen to well represent the finite one. The Lagrangian coefficient of an infinite beam can be easily deduced from Eq. (16). It is constant, equal to $\eta/2$ in the case of force excitation and $-\eta/2$ in the case of moment excitation. The Lagrangian energy of a finite or semi-infinite beam is thus quite different than that of an infinite beam.

Fig. 14 shows the band-averaged Lagrangian coefficient. The frequency averaging was applied to kinetic and potential energies first, and then the Lagrangian coefficient was calculated from the averaged data. Once again the matching between the finite and semi-infinite beam is seen to be very good. The matching with the infinite beam is poor as could have been expected.

It can be concluded that the energy of a long finite beam can be modelled in a frequency-averaged sense by that of an equivalent semi-infinite beam. On the contrary, an infinite beam is not a good representative of a finite beam where energy concepts are concerned.

5. Conclusions

Some generic features of energy and energy flow in thin rods and beams have been investigated. The equations of energy density and energy flow are formulated in terms of wave amplitudes. These equations are exact up to the validity of thin rod and Euler–Bernoulli beam models and up to the assumption of low damping (loss factor squared much smaller than unity). The differential

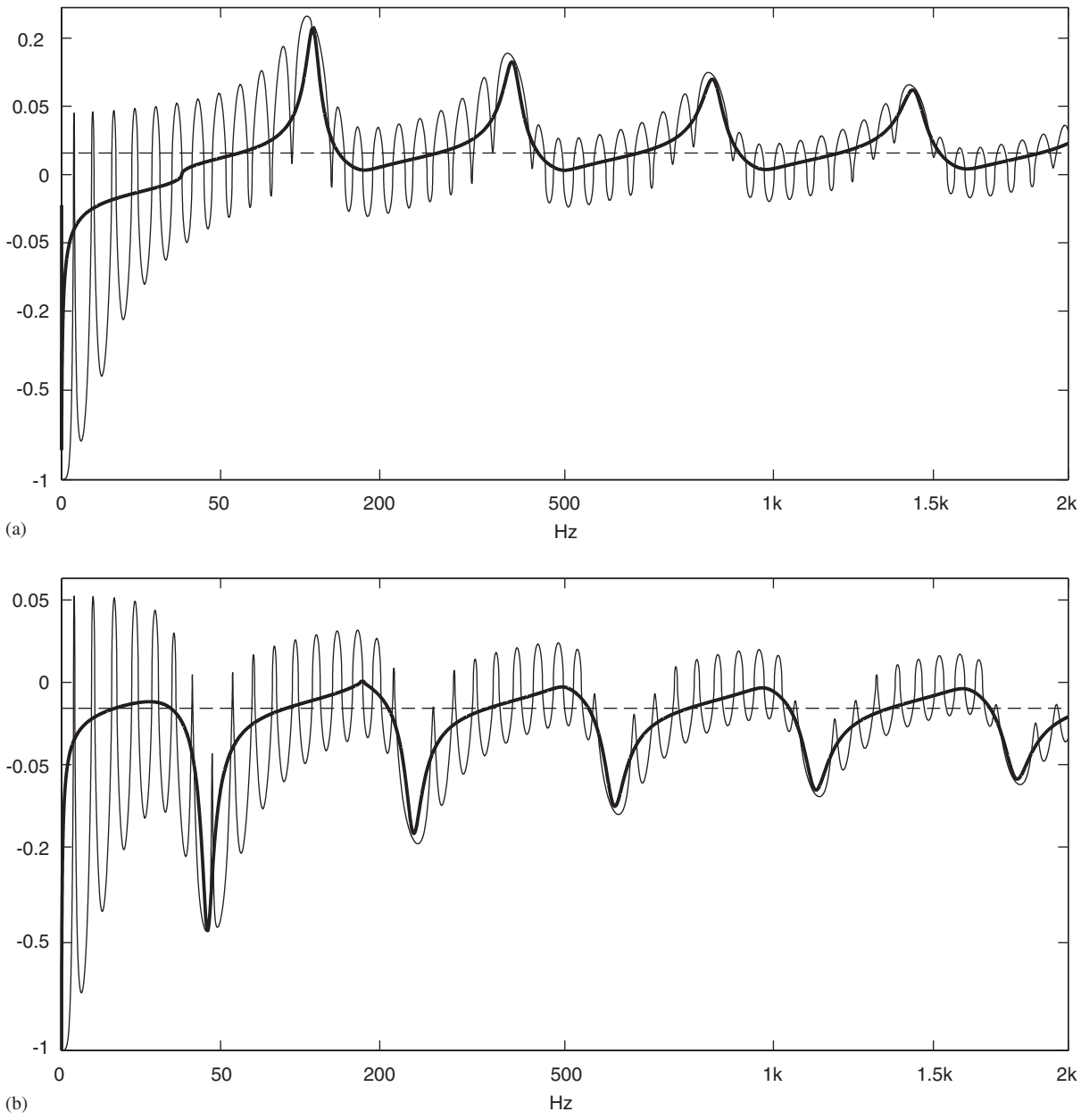

Fig. 13. Lagrangian coefficient of a beam vibrating in flexure: (a) force excitation and (b) moment excitation. Thin line: finite beam; thick line: equivalent semi-infinite beam; dashed line: infinite beam.

equations for energy and energy flow have been formulated in terms of interfering vibration waves. Some discrepancies with an earlier model have been found.

It has been shown that, contrary to kinetic energy density, the potential energy density exhibits a jump at the excitation point of a rod or a moment-driven beam. This feature can be employed

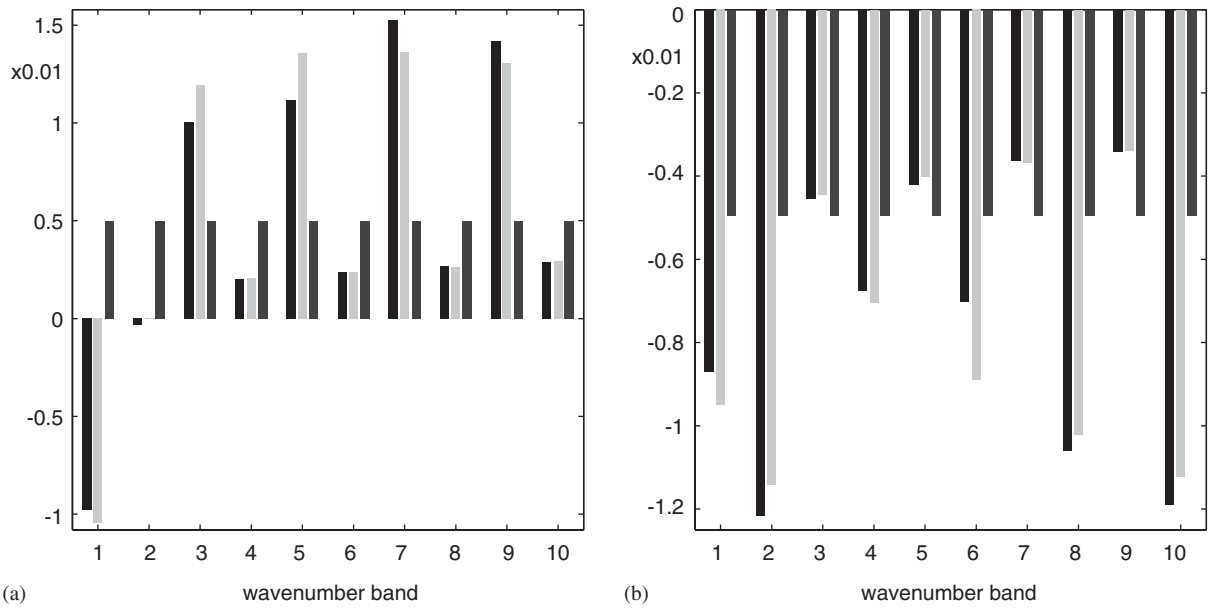

Fig. 14. Lagrangian coefficient of a finite (black), semi-infinite (light grey) and infinite (dark grey) beam obtained by band averaging: (a) unit force excitation and (b) unit moment excitation. Band limits are marked by dotted lines on Fig. 11.

when optimising the placement of damping treatments. Increased attention has been paid to energy features of semi-infinite rods and beams, in particular to the distribution of kinetic and potential energies within the end section, i.e. the section between the excitation and the end positions. The damping was shown to reduce the jump in potential energy across the excitation point, but in turn increases the frequency range of strong power input to the end section.

Finally, a comparison was made of the energy properties of a long finite beam and equivalent semi-infinite and infinite beams. The semi-infinite beam was found to match very well the frequency-averaged energy of the finite beam. On the contrary, the infinite beam shows poor energy matching.

Appendix A. Energy and energy flow in an axially vibrating rod

To account for the damping the elasticity modulus E and thus the wavenumber k are taken complex, [30]

$$E \to E(1+\mathrm{j}\eta) \;\; \therefore \;\; k = \omega/c \to k\Big/\sqrt{1+\mathrm{j}\eta} \approx k(1-\mathrm{j}\eta/2), \tag{A.1}$$

where the right-hand approximation holds for low damping $\eta \ll 1$.

The kinetic and potential energy densities of an axially vibrating rod are simple functions of the axial displacement u. As these quantities are constant across the rod thickness, it is appropriate to use the notion of energy per unit length, i.e. the energy density multiplied by the cross-sectional

area S. Upon inserting complex k in Eq. (2), the kinetic and potential unit energies are readily computed.

The time-averaged unit-length kinetic energy equals (prime denotes a unit-length quantity)

$$\overline{E'_k} = \frac{1}{2}m'\overline{\dot{u}^2} \hat{=} \frac{1}{4}m'\omega^2\left|U^2\right| = \frac{1}{4}m'\omega^2\left[\left|A_+^2\right|\mathrm{e}^{-\eta kx} + \left|A_-^2\right|\mathrm{e}^{\eta kx} + 2\left|A_+\right|\left|A_-\right|\cos(\varphi_+ - \varphi_- - 2kx)\right], \tag{A.2}$$

m' being the unit-length mass of the rod. The mean potential energy density is equal to half the averaged product of axial stress σ_x and axial strain ε_x. The strain–stress–displacement relationship for a rod is a particularly simple one, $\varepsilon_x = \partial u/\partial x$, $\sigma_x = E\varepsilon_x$, yielding the following expression for the unit-length potential energy of a damped rod:

$$\begin{aligned}\overline{E'_p} &= \frac{1}{2}S\overline{\sigma_x\varepsilon_x} \hat{=} \frac{1}{4}S\,\mathrm{Re}(E)\left|\frac{\partial U}{\partial x}\right|^2 \\ &= \frac{1}{4}m'\omega^2\left[\left|A_+^2\right|\mathrm{e}^{-\eta kx} + \left|A_-^2\right|\mathrm{e}^{\eta kx} - 2\left|A_+\right|\left|A_-\right|\cos(\varphi_+ - \varphi_- - 2kx)\right].\end{aligned} \tag{A.3}$$

In Eq. (6b) as well as in the expressions to follow the η^2 terms are neglected in comparison with 1.

The total mean energy density reads

$$\overline{E'} = \overline{E'_k} + \overline{E'_p} = \frac{1}{2}m'\omega^2\left[\left|A_+^2\right|\mathrm{e}^{-\eta kx} + \left|A_-^2\right|\mathrm{e}^{\eta kx}\right]. \tag{A.4}$$

The mean energy density, just like the net intensity, is interference-free, i.e. equals the sum of the energies of two waves taken individually. The energy of each of the two decreases exponentially in the direction of wave travel. While the kinetic and potential energies vary considerably along the rod, due to the contribution of the last term in Eqs. (A.2) and (A.3), the total energy varies slowly.

The mean axial intensity equals the negative product between the axial stress and particle velocity. By multiplying the intensity by the cross-sectional area the energy flow P is obtained. Expressed in complex form, the time-averaged energy flow becomes equal to

$$\begin{aligned}\overline{P} &= -S\overline{\sigma_x\dot{u}} = -\frac{1}{2}SE\frac{\partial U}{\partial x}(\mathrm{j}\omega U)^* \\ &= \frac{1}{2}m'c\omega^2(1+\mathrm{j}\eta/2)\left[\left|A_+^2\right|\mathrm{e}^{-\eta kx} - \left|A_-^2\right|\mathrm{e}^{\eta kx} + 2\mathrm{j}\left|A_+\right|\left|A_-\right|\sin(\varphi_+ - \varphi_- - 2kx)\right].\end{aligned} \tag{A.5}$$

The real part of energy flow, the net flow, varies slowly along the rod:

$$\mathrm{Re}(\overline{P}) = \frac{1}{2}m'c\omega^2\left[\left|A_+^2\right|\mathrm{e}^{-\eta kx} - \left|A_-^2\right|\mathrm{e}^{\eta kx} - \eta\left|A_+\right|\left|A_-\right|\sin(\varphi_+ - \varphi_- - 2kx)\right]. \tag{A.6}$$

By setting damping to zero, Eq. (4) is obtained. In this case the flow is constant.

The imaginary part of complex energy flow reads

$$\mathrm{Im}(\overline{P}) = -\frac{1}{2}m'c\omega^2\left[\frac{\eta}{2}\left(\left|A_+^2\right|\mathrm{e}^{-\eta kx} - \left|A_-^2\right|\mathrm{e}^{\eta kx}\right) + \left|A_+\right|\left|A_-\right|\sin(\varphi_+ - \varphi_- - 2kx)\right]. \tag{A.7}$$

At zero damping the imaginary part varies spatially in a sinusoidal fashion around zero mean value.

The flow divergence can be easily evaluated from Eq. (A.5) as $\partial P/\partial x$:

$$\nabla(\overline{P}) = -\frac{1}{2}m'\omega^3(1+\mathrm{j}\eta/2)\big[\eta\big(|A_+^2|\mathrm{e}^{-\eta kx}+|A_-^2|\mathrm{e}^{\eta kx}\big) + 4\mathrm{j}|A_+||A_-|\cos(\varphi_+-\varphi_--2kx)\big]. \tag{A.8}$$

Its real part

$$\mathrm{Re}\{\nabla(\overline{P})\} = -\frac{1}{2}m'\omega^3\eta\big[|A_+^2|\mathrm{e}^{-\eta kx}+|A_-^2|\mathrm{e}^{\eta kx} - 2|A_+||A_-|\cos(\varphi_+-\varphi_--2kx)\big]. \tag{A.9}$$

representing the energy loss per unit length contains η as a common factor. It is easy to prove that the term in brackets of Eq. (A.9) can never be negative, thus the divergence is always negative indicating loss of energy at all positions vibrating freely according to Eq. (2).

By comparing Eq. (A.8) with Eqs. (A.2) and (A.3) the validity of Eq. (1) is confirmed. It is worth noting that Eqs. (A.2)–(A.8) were derived from the solution of the wave equation, while Eq. (1) was derived from the consideration of an elementary volume of a solid body.

Appendix B. Energy and energy flow in a beam vibrating in flexure

The instantaneous potential and kinetic energies per unit length of a beam vibrating in flexure read

$$E_k' = \frac{1}{2}m'\dot{u}^2, \qquad E_p' = \frac{1}{2}B\left|\frac{\partial^2 u}{\partial x^2}\right|^2. \tag{B.1}$$

The energy flow in a beam vibrating in flexure is created by the internal work of the shear force Q and the bending moment M. Its instantaneous value is

$$P = Q\dot{u} + M\frac{\partial\dot{u}}{\partial x} = B\left[\frac{\partial^3 u}{\partial x^3}\dot{u} - \frac{\partial^2 u}{\partial x^2}\frac{\partial\dot{u}}{\partial x}\right]. \tag{B.2}$$

Assuming lossless material, i.e. real flexural stiffness B, the formula above applied to the wave solution (9) yields a simple expression for net power (Eq. (10)). By admitting damping through complex stiffness B and thus k, an equivalent formula can be established for the complex power using Eqs. (9), (11) and (B.2)

$$\overline{P} = \frac{m'\omega^3}{k}(1+\mathrm{j}\eta/2)(S_r+\mathrm{j}S_i). \tag{B.3}$$

Here S_r and S_i are real-valued functions depending on different combinations of amplitude products:

$$\begin{aligned}
S_r &= \left|A_+^2\right|\mathrm{e}^{-\eta kx/2} - \left|A_-^2\right|\mathrm{e}^{\eta kx/2} - 2\left|C_+\right||C_-|\sin(\psi_+ - \psi_- + \eta kx/2) \\
&\quad + \eta/4\left[\left|C_+^2\right|\mathrm{e}^{-2kx} - \left|C_-^2\right|\mathrm{e}^{2kx} + 2\left|A_+\right||A_-|\sin(\varphi_+ - \varphi_- - 2kx)\right], \\
S_i &= \sqrt{2}(1-\eta/4)\left|A_+\right|\left|C_+\right|\mathrm{e}^{-k(1+\eta/4)x}\cos[\varphi_+ - \psi_+ - k(1+\eta/4)x - \pi/4] \\
&\quad - \sqrt{2}(1+\eta/4)\left|A_+\right||C_-|\mathrm{e}^{k(1-\eta/4)x}\cos[\varphi_+ - \psi_- - k(1-\eta/4)x + \pi/4] \\
&\quad + \sqrt{2}(1+\eta/4)|A_-|\left|C_+\right|\mathrm{e}^{-k(1-\eta/4)x}\cos[\varphi_- - \psi_+ + k(1-\eta/4)x + \pi/4] \\
&\quad - \sqrt{2}(1-\eta/4)|A_-||C_-|\mathrm{e}^{k(1+\eta/4)x}\cos[\varphi_- - \psi_- + k(1+\eta/4)x - \pi/4].
\end{aligned} \tag{B.3a}$$

It should be recalled that C_+ and C_- represent the amplitudes of evanescent waves at the same position, i.e. $x = 0$ (Eq. (9)). The evanescent waves have maximum amplitudes at the beam ends from which the waves decay. These amplitudes are usually of the same order of magnitude as the amplitudes of the propagating waves, or smaller. Thus, the product of C_+ and C_- will be negligible at all but very low frequencies where the length of the beam is shorter than the vibration wavelength. For the same reason the terms containing $|C_+|$ and $|C_-|$ will be negligible at positions away from the beam ends. Close to one of the two ends only one of these terms can be important.

By examining Eq. (B.3) and taking the last comments into account it can be easily concluded that the real part of energy flow will be dominated by the S_r factor which can be further simplified for use at mid- and high-frequencies by suppressing its evanescent terms:

$$\mathrm{Re}\{\overline{P}\} \approx \frac{m'\omega^3}{k} S_r, \tag{B.3b}$$

$$S_r \approx \left|A_+^2\right|\mathrm{e}^{-\eta kx/2} - \left|A_-^2\right|\mathrm{e}^{\eta kx/2} + \eta/2\left|A_+\right||A_-|\sin(\varphi_+ - \varphi_- - 2kx). \tag{B.3c}$$

Eq. (B.3) further shows that the imaginary part of energy flow will be contributed substantially not only by the S_r factor but by the S_i factor as well. The coupling between the propagating and evanescent waves thus is not negligible in this case.

The energy flow divergence is then obtained as (η^2 terms neglected in comparison with unity)

$$\nabla \cdot \overline{P} = \partial\overline{P}/\partial x = -m'\omega^3(1 + \mathrm{j}\eta/2)(G_r + \mathrm{j}G_i), \tag{B.4}$$

$$\begin{aligned}
G_r &= \eta/2\Big[\left|A_+^2\right|\mathrm{e}^{-\eta kx/2} + \left|A_-^2\right|\mathrm{e}^{\eta kx/2} + \left|C_+^2\right|\mathrm{e}^{-2kx} + \left|C_-^2\right|\mathrm{e}^{2kx} \\
&\quad + 2\left|A_+\right||A_-|\cos(\varphi_+ - \varphi_- - 2kx) + 2\left|C_+\right||C_-|\cos(\psi_+ - \psi_- + \eta kx/2)\Big], \\
G_i &= 2\left|A_+\right|\left|C_+\right|\mathrm{e}^{-k(1+\eta/4)x}\cos[\varphi_+ - \psi_+ - k(1+\eta/4)x] \\
&\quad + 2\left|A_+\right||C_-|\mathrm{e}^{k(1-\eta/4)x}\cos[\varphi_+ - \psi_- - k(1-\eta/4)x] \\
&\quad + 2|A_-|\left|C_+\right|\mathrm{e}^{-k(1-\eta/4)x}\cos[\varphi_- - \psi_+ + k(1-\eta/4)x] \\
&\quad + 2|A_-||C_-|\mathrm{e}^{k(1+\eta/4)x}\cos[\varphi_- - \psi_- + k(1+\eta/4)x].
\end{aligned} \tag{B.4a}$$

Omitting the proof for the sake of brevity, the fundamental relationship between energy and energy flow, given by Eq. (1), can be shown to fully apply in this case

$$\mathrm{Re}(\nabla \cdot \overline{P}) = -2\omega\eta\overline{E'_p} \Rightarrow \overline{E'_p} = \frac{m'\omega^2}{2}\left(\frac{G_r}{\eta} - \frac{G_i}{2}\right),$$
$$\mathrm{Im}(\nabla \cdot \overline{P}) = -2\omega(\overline{E'_k} - \overline{E'_p}) \Rightarrow \overline{E'_k} \cong \frac{m'\omega^2}{2}\left(\frac{G_r}{\eta} + \frac{G_i}{2}\right). \tag{B.5}$$

In the last expression η^2 has been again neglected in comparison with unity.

The total energy density of the flexurally vibrating beam thus equals

$$\overline{E'} = \overline{E'_p} + \overline{E'_k} = \frac{m'\omega^2}{\eta} G_r. \tag{B.6}$$

It can be seen that the coupling between the propagating and evanescent waves, contained in the G_i factor, does not affect the total energy density. This factor does, however, appear in the explicit expressions for kinetic and potential energies (Eq. (B.5)), but with opposite sign thus cancelling itself from the sum of the two.

Eq. (B.7) indicates that the G_i factor governs the difference of kinetic and potential energy densities, i.e. the Lagrangian energy density:

$$\overline{L'} = \overline{E'_k} - \overline{E'_p} \cong \frac{m'\omega^2}{2} G_i. \tag{B.7}$$

Thus, the difference of kinetic and potential energy densities in a beam comes mainly for the interference between the propagating and evanescent waves. It follows that this difference will increase near the ends and excitation zones and will disappear in the interior free zones.

References

[1] D.U. Noiseux, Measurement of power flow in uniform beams and plates, *Journal of the Acoustical Society of America* 47 (1970) 238–247.

[2] G. Pavić, Measurement of structure borne wave intensity, part I: formulation of methods, *Journal of Sound and Vibration* 49 (1976) 221–230.

[3] J.W. Verheij, Cross-spectral density methods for measuring structure-borne power flow on beams and pipes, *Journal of Sound and Vibration* 70 (1980) 133–139.

[4] J. Linjama, T. Lahti, Estimation of bending wave intensity in beam using the frequency response technique, *Journal of Sound and Vibration* 153 (1992) 21–36.

[5] G. Pavić, Vibroacoustical energy flow through straight pipes, *Journal of Sound and Vibration* 154 (1992) 411–429.

[6] C.R. Halkyard, B.R. Mace, A wave component approach to structural intensity in beams, *Proceedings of the Fourth International Congress on Intensity Techniques*, Senlis, August–September 1993, pp. 183–190.

[7] G. Pavić, Accuracy of energy flow measurement in pipes using the wave de-composition technique, *Proceedings of the Fourth International Congress on Intensity Techniques*, Senlis, August–September 1993, pp. 191–198.

[8] J. Pan, R. Ming, C.H. Hansen, R.L. Clark, Experimental determination of the total vibratory power transmission in an elastic beam, *Journal of the Acoustical Society of America* 104 (1998) 898–906.

[9] R. Szwerc, C.B. Burroughs, S.A. Hambric, T.E. McDevitt, Power flow in coupled bending and longitudinal waves in beams, *Journal of the Acoustical Society of America* 107 (2000) 3186–3195.

[10] P.D. Bauman, Measurement of structural intensity: analytic and experimental evaluation of various techniques for the case of flexural waves in one dimensional structures, *Journal of Sound and Vibration* 174 (1994) 677–694.
[11] C.R. Halkyard, B.R. Mace, Structural intensity in beams—waves, transducer systems and the conditioning problem, *Journal of Sound and Vibration* 185 (1995) 279–298.
[12] J.R.F. Arruda, J.P.R. Campos, J.I. Piva, Experimental determination of flexural power flow in beams using a modified Prony method, *Journal of Sound and Vibration* 197 (1996) 309–328.
[13] J.R.F. Arruda, J.P.R. Campos, J.I. Piva, Measuring flexural power flow in beams using a spatial-domain regressive discrete Fourier series, *Proceedings of the 21st International Conference on Noise and Vibration Engineering*, Leuven, 1996, pp. 641–652.
[14] C.R. Fuller, G.P. Gibbs, R.J. Silcox, Simultaneous active control of flexural and extensional power flow in beams, *Journal of Intelligent Material Systems and Structures* 1 (1990) 235–247.
[15] V.D. Belov, S.A. Rybak, Applicability of the transport equation in one-dimensional wave-propagation problem, *Soviet Physics—Acoustics* 21 (1975) 110–114.
[16] V.D. Belov, S.A. Rybak, B.D. Tartakovskii, Propagation of vibrational energy in absorbing structures, *Soviet Physics—Acoustics* 23 (1977) 115–119.
[17] L.E. Buvailo, A.V. Ionov, Application of the finite-element method to the investigation of the vibroacoustical characteristics of structures at high audio frequencies, *Soviet Physics—Acoustics* 26 (1980) 277–279.
[18] D.J. Nefske, S.H. Sung, Power flow finite element analysis of dynamic systems: basic theory and applications to beams, *Journal of Vibration, Acoustics, Stress and Reliability in Design* 111 (1989) 94–100.
[19] J.C. Wohlever, R.J. Bernhard, Mechanical energy flow models in rods and beams, *Journal of Sound and Vibration* 153 (1992) 1–19.
[20] A. Carcaterra, A. Sestieri, Energy density equations and power flow in structures, *Journal of Sound and Vibration* 188 (1995) 269–282.
[21] Y. Lase, M.N. Ichchou, L. Jezequel, Energy flow analysis of bars and beams: theoretical formulations, *Journal of Sound and Vibration* 192 (1996) 281–305.
[22] A. Le Bot, Energy Equations in Mechanical Vibration: Application to Medium and High Frequencies, Doctoral Thesis, L'Ecole Centrale de Lyon, 1994 (in French).
[23] Ph.E. Cho, R.J. Bernhard, Energy flow analysis of coupled beams, *Journal of Sound and Vibration* 211 (1998) 593–605.
[24] C. Soize, A model and numerical method in the medium frequency range for vibroacoustic predictions using the theory of structural fuzzy, *Journal of the Acoustical Society of America* 94 (1993) 849–865.
[25] R.S. Langley, P. Bremner, A hybrid method for the vibration analysis of complex structural-acoustic systems, *Journal of the Acoustical Society of America* 105 (1999) 1657–1671.
[26] B.R. Mace, P.J. Shorter, Energy flow models from finite element analysis, *Journal of Sound and Vibration* 233 (2000) 369–389.
[27] G. Pavić, Numerical study of vibration damping, energy and energy flow in a beam–plate system, *Journal of Sound and Vibration*, 2006, in press (doi:10.1016/j.jsv.2005.07.020).
[28] J. Liang, B.A.T. Petersson, Estimation of vibration distribution for finite structures, *Journal of Sound and Vibration* 238 (2000) 271–293.
[29] G. Pavić, The role of damping on energy and power in vibrating systems, *Journal of Sound and Vibration* 281 (2005) 45–71.
[30] L. Cremer, M. Heckl, E.E. Ungar, *Structure-borne Sound*, Springer, Berlin, 1973.
[31] B.A.T. Petersson, Structural acoustic power transmission by point moment and force excitation, part I: beam- and frame-like structures, *Journal of Sound and Vibration* 160 (1993) 43–66.
[32] H.G.D. Goyder, R.G. White, Vibrational power flow from machines into built-up structures; part I, *Journal of Sound and Vibration* 68 (1980) 59–75.
[33] E. Skudrzyk, *Simple and Complex Vibratory Systems*, Pennsylvania State University Press, University Park, 1968.